ENGINEERING-PDH.com
ONLINE CONTINUING EDUCATION

GEARBOX RELIABILITY ANALYSIS OF A WIND TURBINE GEARBOXES

Main Category:	Mechanical Engineering
Sub Category:	-
Course #:	MEC-151
Course Content:	71 pgs
PDH/CE Hours:	5

COURSE/EXAM PREVIEW
(HIT BACK TO RETURN TO ENGINEERING-PDH.COM)

MEC-151 EXAM PREVIEW

Instructions:

- Review the course & exam preview below.
- Click "Add to Cart" from the course page on the website. You can "Continue Shopping" to add additional courses, or checkout. Don't forget to apply your coupon code if you have one before checkout.
- After checkout you will be provided with links to download the official courses/exams.
- At your convenience and own pace, you can review the course material. When ready, select "Take Exam" to complete the live graded exam. Don't worry, you can take an exam as many times as needed to pass.
- Upon a satisfactory completion of the course exam, which is a score of 70% or better, you will be provided with your course completion certificate. Be sure to download and print your certificates to keep for your records.

Exam Preview:

1. The data were recorded in two separate data streams by acquisition rate. A 100-hertz (Hz) rate was used to record information on the planetary and intermediate sections of the gearbox. A 2,000-Hz rate was used to record information on the high-speed section of the gearbox.
    a. True
    b. False
2. According to the reference material, the gearbox is composed of one low-speed planetary stage that accommodates ____ planet gears, and two parallel shaft stages.
    a. 2
    b. 3
    c. 4
    d. 5
3. The NWTC 2.5-megawatt (MW) dynamometer test facility was used for Phase 3 testing. The new drive uses a voltage source converter topology, enabling dynamic torque control via Profibus DP up to a bandwidth of ____ Hz.
    a. 60
    b. 120
    c. 180
    d. 250
4. The maximum acquisition rate that the DAS can record simultaneous data across the multiple backplanes used for GRC instrumentation is just above 20 kHz.
    a. True
    b. False

5. According to the refence material, _____ strain gauges were mounted in axial grooves in the inner races of the planet bearings to provide information on planet loads and roller contact pressure distribution.
    a. 12
    b. 24
    c. 36
    d. 48

6. At the HSS once-per-revolution frequency, the signals are within 6% of each other; at the outer race roller passage frequency they are within 14% of each other.
    a. True
    b. False

7. According to the reference material, at full speed the HSS is rotating at 30 Hz, or ____ rpm. In conjunction with the properties of the 32222 J2 TRB, this results in an outer race roller passage frequency of 254.7 Hz.
    a. 1500
    b. 1800
    c. 2000
    d. 2200

8. Using Table 1. Gearbox Run-In Procedure, what was the longest duration gearbox run-in that was conducted during the study?
    a. 1.0 hour
    b. 1.5 hours
    c. 2.5 hours
    d. 4.5 hours

9. Normal power production cases representing 15-meters per second (m/s), 25-m/s, and 35-m/s wind speed cases were tested. In each case, a system identification test was performed in which the desired dynamic torque is commanded, and the actual torque is measured.
    a. True
    b. False

10. According to section 4.2.2 of the reference material, during testing, it was discovered that these gauges had been installed on a ___° helix angle instead of the proper 7.5° helix angle of the ring gear, and with an incorrect position reference.
    a. 9.5
    b. 12.5
    c. 14
    d. 17.5

List of Acronyms

CRB	cylindrical roller bearing
DAS	data acquisition system
deg	degree of rotation
DW	downwind
FO	fiber optic
GB	gearbox
GRC	Gearbox Reliability Collaborative
HSS	high-speed shaft
ISS	intermediate-speed shaft
kVAR	kilovolt-ampere reactive
LSS	low-speed shaft
LVDT	linear variable displacement transducer
mV/V	millivolts per volt
NI	National Instruments
NREL	National Renewable Energy Laboratory
NTL	nontorque load
NWTC	National Wind Technology Center
RTD	resistance temperature detector
stbd	starboard
TRB	tapered roller bearing
UW	upwind
VDC	volts direct current
VFD	variable frequency drive

GEARBOX EXAMINATION #1

1 Introduction and Background

Many gearboxes in wind turbines have not been achieving their expected design life [1]; they do, however, commonly meet or exceed the design criteria specified in current standards in the gear, bearing, and wind turbine industry as well as third-party certification criteria. The cost of gearbox replacements and rebuilds, as well as the downtime associated with these failures, has elevated the cost of wind energy. In 2006, the U.S. Department of Energy established the National Renewable Energy Laboratory (NREL) Gearbox Reliability Collaborative (GRC). Its key goal is to understand the root causes of premature gearbox failures and improve their reliability [2]. The GRC is examining a hypothesis that the gap between design-estimated and actual wind turbine gearbox reliability is caused by underestimation of loads, inaccurate design tools, the absence of critical elements in the design process, or insufficient testing.

The GRC uses a combined gearbox testing, modeling, and analysis approach. The collaborative disseminates data and results to the industry, facilitating gearbox reliability improvement. Full-scale dynamometer testing builds an understanding of how selected loads and events translate into gear and bearing response, including reactions, load distributions, displacements, temperatures, stresses, and slip. Ideally, the knowledge gained from the GRC will result in any necessary improvements to gearbox design standards and associated modeling tools.

This test report describes the recent tests of GRC gearbox (GB) 2 in the National Wind Technology Center (NWTC) dynamometer and documents any modifications to the original test plan [3]. In this manner, it serves as a guide for interpreting the publicly released data sets with brief analyses to illustrate the data. Specific objectives of the test were to assess the effect of dynamic nontorque load (NTL) on the planetary section, generator misalignment on the high-speed shaft (HSS), and field representative conditions on the gearbox in general. Detailed analysis of those test objectives will be presented in subsequent publications.

1

2 Test Article

The GRC test article drivetrain was originally designed for a two-speed, stall-controlled, three-bladed upwind turbine with a rated power of 750 kilowatts (kW) [2]. The design follows a conventional configuration in which all the drivetrain components are mounted onto the bed plate. These components include the hub, main bearing, main shaft, gearbox, brake, generator shaft, and generator (see Figure 1). Everything but the hub is included in the dynamometer tests. The drivetrain follows a common configuration of megawatt-scale turbines used in the industry today. The gearbox is mounted with a three-point configuration in which torsional loads are transferred to the main frame through two torque arms, and forces are reacted mostly at the main bearing.
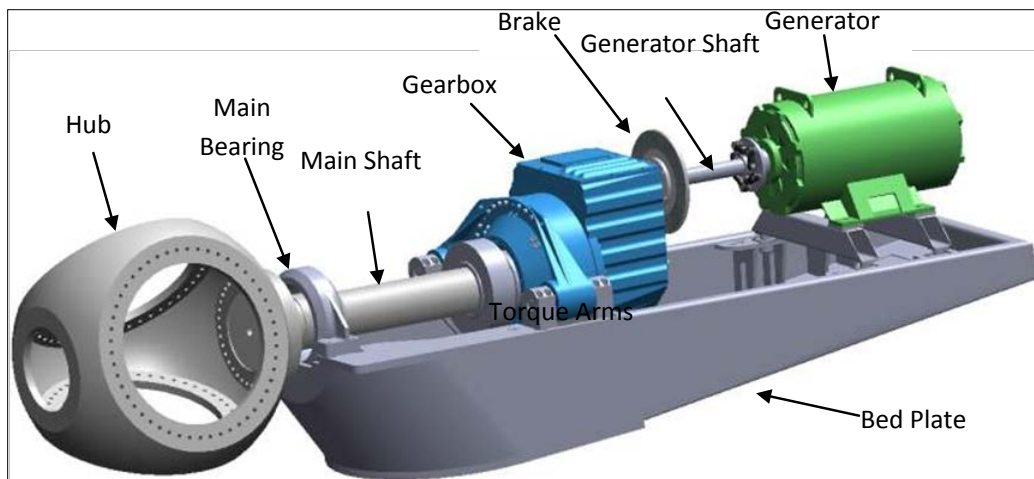

Figure 1. Drivetrain configuration

The gearbox is composed of one low-speed planetary stage that accommodates three planet gears, and two parallel shaft stages (see Figure 2). The gears and bearings were redesigned and have been modified from the original gearbox configuration used in the commercial versions of this wind turbine. From this point forward, the redesigned gearbox is referred to as the "the GRC gearbox."
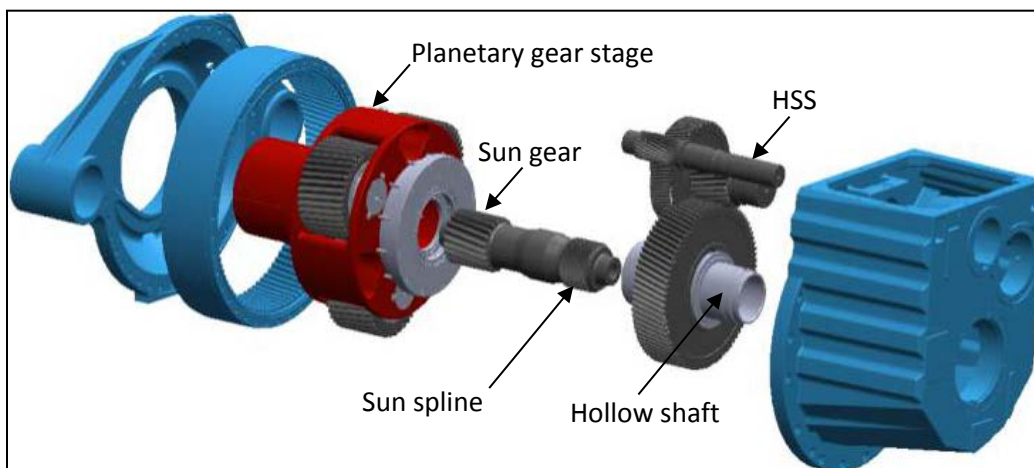

Figure 2. Gearbox configuration. *Illustration by Powertrain Engineers Inc.*

2

2.1 High-Speed Shaft Installation

Feedback from GRC partners highlighted the need for measurements of gear and bearing response on the HSS because of the high rate of failures and subsequent repair costs for these bearings in the industry [1,4]. The reliability of this bearing configuration remains a weak link because of a possible disconnect between the actual loading behavior and the loading behavior assumed by the design. HSS bearings in wind turbine gearboxes can be subject to low loads at high speeds, torque transients, and even torque reversals. When rollers enter and leave the shifting load zone during such events, they are prone to skidding that can lead to surface distress and damage [5].

In the GRC Phase 3, instrumentation was added to measure the HSS bending, torque, pinion tooth load distribution, and radial load distribution and temperature of the locating tapered roller bearing (TRB) pair [3]. One of the main goals of Phase 3 testing is to assess these loads in normal operation, generator misalignment, and simulated stop conditions. As shown in Figure 3, the HSS is supported by a cylindrical roller bearing (CRB) upwind and a close-coupled TRB pair mounted in an O-configuration downwind of the gear mesh.
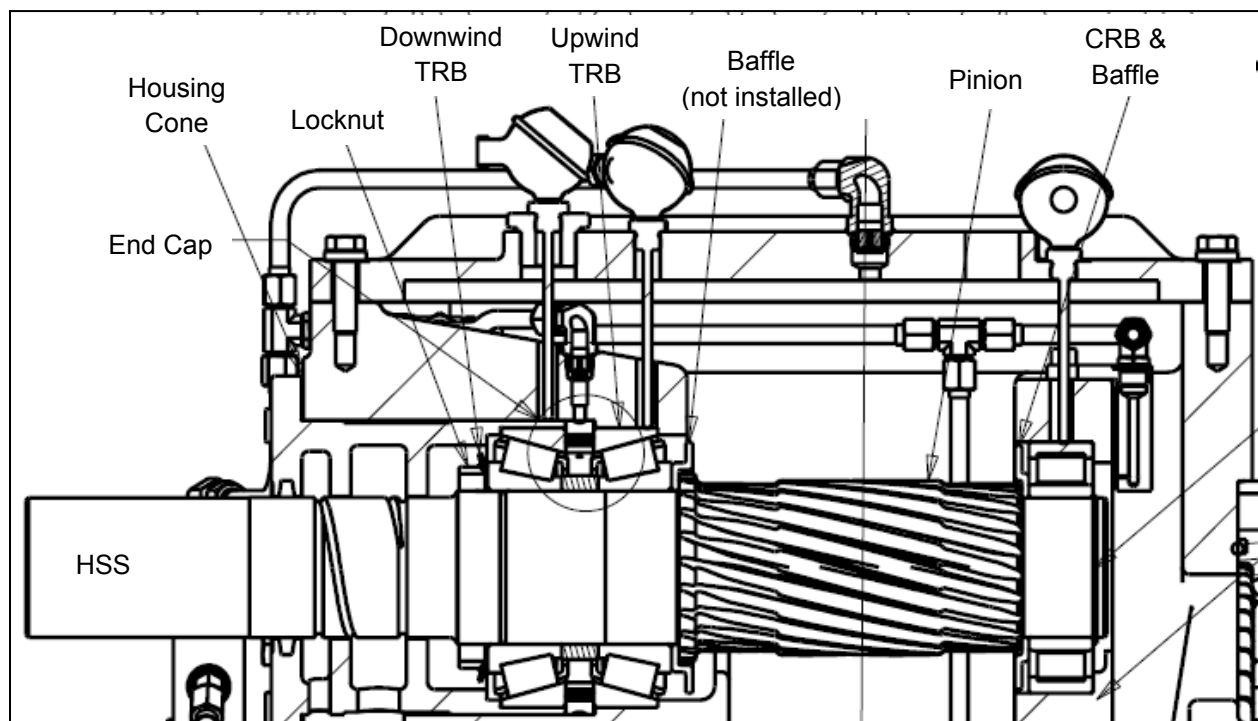

Figure 3. Schematic of HSS installation in the gearbox [6]. *Illustration by Powertrain Engineers Inc.*

Because the primary objective of Phase 3 testing of GB2 is to measure HSS, pinion, and bearing loads, it is important to note two important differences between the gearbox drawings and the actual installation [6]. Both of these items have been present since the GB2 was originally built, although they have become relevant only in Phase 3. These two differences follow:

- The baffle (P/N 251559) just upwind of the TRB pair was never installed. The baffle is 5 mm thick, so when it is omitted the TRB pair is 5 mm farther upwind on the shaft itself.

3

- The counterbore inside the gearbox housing (P/N 251342) is deeper than specified. It was specified as 254 mm, but it is actually 260.8 mm. This counterbore was intended to locate the HSS assembly axially. This means that when the HSS assembly is inserted into the gearbox, it was intended to slide forward to the point at which the outer ring of the upwind TRB meets the counterbore lip, leaving a 1-mm axial gap in between the TRB spacer and the housing. Because the counterbore is too deep, the HSS assembly is instead axially located by this latter feature. In other words, the HSS assembly actually slid forward to the point at which the TRB spacer met the counter-bore lip at 209 mm, leaving no axial gap. As a result, the HSS assembly is 1 mm farther upwind than intended.

The net effects, relative to the drawings, follow:

- The TRB pair is located 1 mm farther *upwind* relative to the housing, and 5 mm farther *upwind* relative to the HSS shaft. Furthermore, the upwind TRB is not restrained axially; there is a 5- to 6-mm axial gap in between it and the housing.

- The HSS is 4 mm farther *downwind* relative to the housing, resulting in two effects. First, the pinion is not centered on the high-speed gear by this amount, compared to the 120-mm face width of this mating gear pair. Second, the CRB rollers are offset from the shaft by 4 mm. This offset increases edge loading of the CRB rollers and CRB inner race.

Figure 4 illustrates these differences. The gearbox designer was consulted about any implications relative to the gearbox operation. For short-term dynamometer testing, these slight differences were deemed to have a minimal impact. For detailed engineering analysis, however, especially the high-speed pinion face width load distribution and the HSS bending moments, these differences were deemed large enough to be accounted for in the gearbox models that are to be compared to the experimental data.
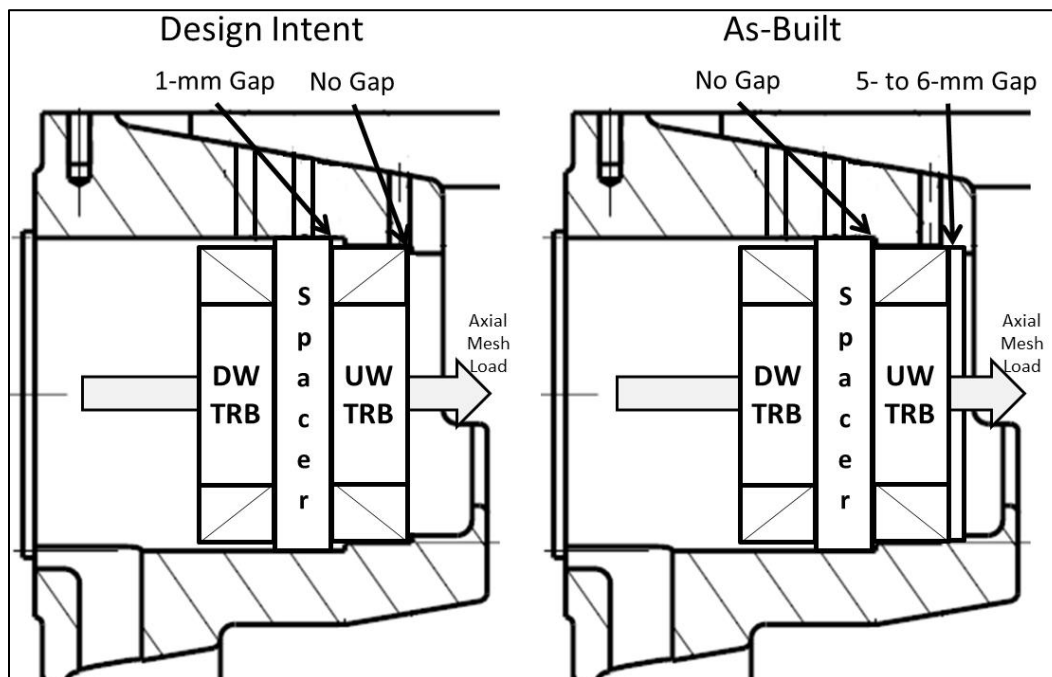

Figure 4. The effect of the deep counterbore in the HSS housing [6]

4

3 Test Environment

3.1 Dynamometer Configuration

The NWTC 2.5-megawatt (MW) dynamometer test facility [7] was used for Phase 3 testing (see Figure 5). The dynamometer variable frequency drive (VFD) was upgraded to an ABB ACS2000 drive [8] before Phase 3 testing started, which is an enabling factor for the reproduction of field condition tests. The new drive uses a voltage source converter topology, enabling dynamic torque control via Profibus DP up to a bandwidth of 250 Hz.

The NTL system is used to apply thrust force, pitch moment, and yaw moments. The system can apply loads statically or dynamically approximately up to 10 Hz depending on force and volume requirements.
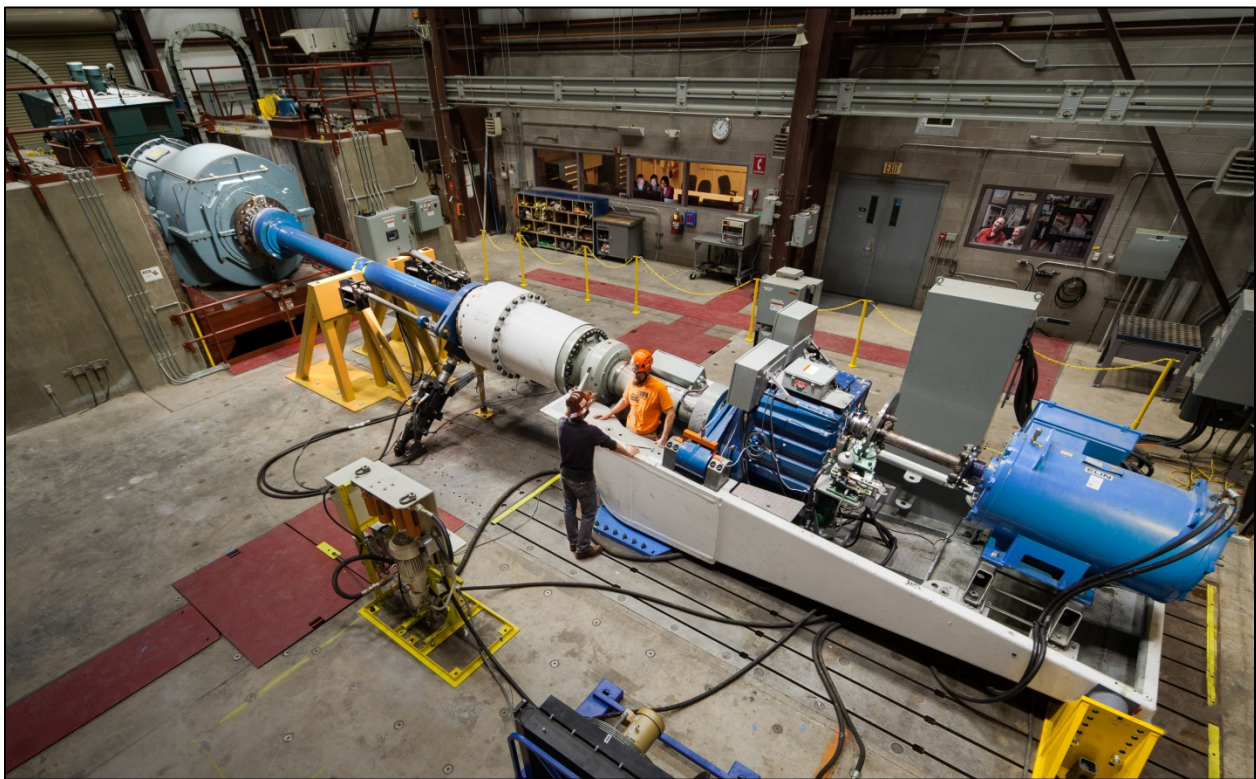

Figure 5. GRC setup. *Photo by Mark McDade, NREL 32734*

The electrical interconnection of the GRC drivetrain to the dynamometer building was also modified from previous testing. Figure 20 in the Appendix presents an updated one-line drawing.

3.2 Lubrication and Cooling Systems

The gearbox lubrication system was significantly simplified before Phase 3 testing to improve its performance. Figure 21 in the Appendix shows a schematic of the system. The oil is pumped by a 3-horsepower (hp) variable speed pump with three inline filters and a pressure-controlled bypass line. The oil is air cooled by a 5-hp fan. The pump and the oil cooler are controlled by their own individual VFDs. Figure 21 in the Appendix does not show the glycol cooling system and fan for the generator.

5

3.3 Data Acquisition System

The data acquisition system (DAS) is based on the National Instruments (NI) deterministic Ethernet platform. Figure 6 shows a general layout of the DAS. One system consisting of two backplanes, which processes rotating frame signals generated on the main shaft and carrier assembly, is mounted to the low-speed shaft (LSS). Figure 22 in the Appendix shows the configuration for this LSS DAS box. The output of that system is converted to fiber optic (FO) and sent across an FO rotary joint to the nonrotating frame. On top of the gearbox, a second system is mounted with two more deterministic Ethernet backplanes, which synchronize the different modules, in separate boxes. These two boxes primarily process fixed-frame signals, but also process some rotating system signals from the HSS. Figure 23 and Figure 24 in the Appendix show the configurations for the port and starboard DAS boxes.
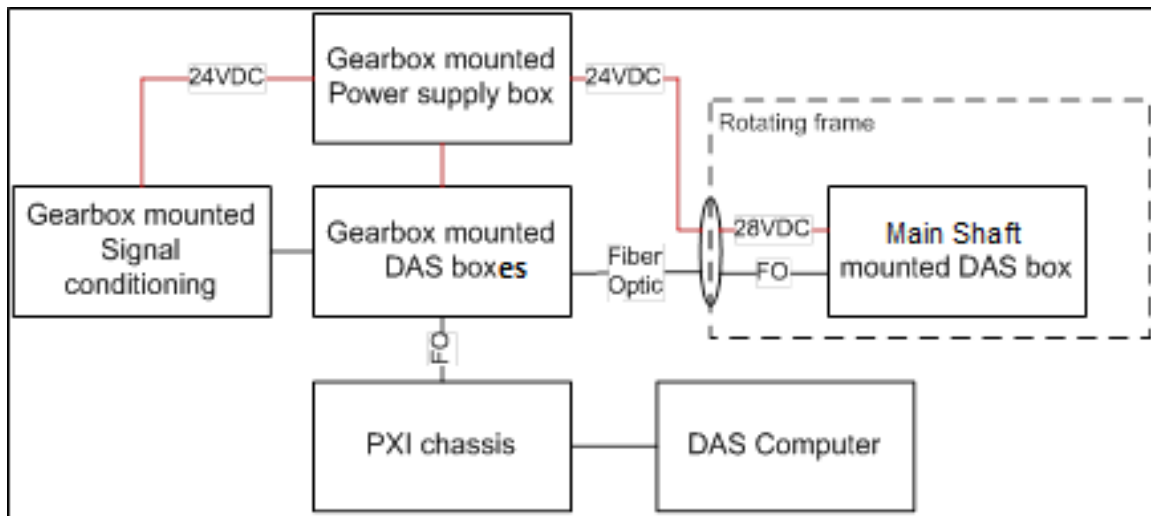

Figure 6. Schematic of GRC data acquisition system

4 Instrumentation

Instrumentation for Phase 3 testing of GB2 was described in detail in the Phase 3 test plan [3]. When the drivetrain was installed and commissioned, however, a number of changes were made for a variety of reasons. Some sensors were found to be nonoperational; others were no longer deemed necessary. The following sections describe these changes. The final section summarizes the signal list.

4.1 Main Shaft

The main shaft signals measured using the encoder were routed through a new signal conditioning device, as shown in Figure 25 in the Appendix. The DAS was configured to calculate main shaft speed (signal name LSS_Speed), from the measured main shaft period (signal name LSS_Period).

During Phase 3 a scaling error was noted in converting the main shaft azimuth (signal name LSS_Azimuth), to engineering units of degrees. The scale factor was corrected in November 2014 so that the signal ranges from 0º to 360º. Before this, the recorded LSS_Azimuth signals were only scaled to reach just above 351º. LSS_Azimuth values measured before November 2014 can be corrected simply by multiplying by a factor of 1.024. At this point, the DAS was also configured to calculate the total main shaft bending moment (signal name MSBM), and fixed-frame bending moments (signal names MSBM_yy and MSBM_zz), from the measured bending moments in the rotating frame (signal names MSBM_YY and MSBM_ZZ), and the main shaft azimuth. The total and fixed-frame moments were useful to set desired testing conditions using the NTL system.

The main shaft axial proximity sensor referenced in the test plan (signal name MS_Axial), was not installed. This sensor was deemed redundant because the three sensors used to measure the carrier motion could be used to determine the relative motion between the main shaft and gearbox. In addition, the set of six sensors used to measure the gearbox motion described in the next section could also be used to determine the absolute motion of the main shaft relative to the stationary mainframe.

4.2 Gearbox

4.2.1 Housing

Motion of the gearbox relative to the mainframe in six degrees of freedom was measured; however, the gearbox vertical motion (signal names Trunion_Z_stbd and Trunion_Z_port), was measured with a linear variable displacement transducer (LVDT) instead of a proximity sensor. The gearbox rotation (signal name Trunion_My_bottom), was measured with a new proximity sensor. Figure 26 and Figure 27 in the Appendix show updated signal sheets for these sensors.

The two triaxial and one uniaxial gearbox accelerometers referenced in the test plan (signal names ACC_port and ACC_stbd), were considered to be redundant with the dedicated condition monitoring accelerometers and were not installed.

4.2.2 Ring Gear

On its inner surface, the ring gear has strain gauges mounted in the root of the internal teeth arranged to sense tooth-bending strain at three circumferential locations. Unfortunately, only the gauges at the top of the gearbox (signal names Ring_0 and Ring_0A) survived all testing entirely intact. Signals Ring_120 and Ring_120A were faulty from the start of Phase 3 testing. Signal Ring_240A ceased to function as a full bridge in April 2014 and was repaired into a half bridge in August 2014 as annotated in Figure 24 in the Appendix.

On its external surface, the ring gear had one set of eight strain gauges installed in an arrangement similar to the internal gauges to measure the tooth-face-width load distribution from the exterior of the ring gear. The corresponding signal names are EXT_KHB followed by a numerical position indicator. During testing, it was discovered that these gauges had been installed on a 14° helix angle instead of the proper 7.5° helix angle of the ring gear, and with an incorrect position reference. As a result, all previous data from Phase 1, Phase 2, and the beginning of Phase 3 are invalid. The existing gauges were removed and new gauges were installed and then verified as operational in August 2014. The naming convention for the gauges was changed as shown in the updated signal sheet in Figure 28 in the Appendix. Note that the true axial position of the gauges along the ring gear face width must be determined by adding the dimension of the recessed area of the ring gear (20 mm) to the position of each gauge.

In addition, the four sets of two gauges on the external surface of the ring gear (signal name RING_LOCAL with a corresponding circumferential reference), were discovered to be damaged before Phase 3 testing resumed. They were not repaired because the existing data from Phase 1 and 2 were deemed to be sufficient.

4.2.3 Planetary Bearings

Thirty-six strain gauges were mounted in axial grooves in the inner races of the planet bearings to provide information on planet loads and roller contact pressure distribution. Three grooves were machined into each bearing. Each groove has two strain gauge pairs arranged in a Poisson configuration—one pair at 25% and one pair at 75% of the inner ring width. All six bearings have a groove at top dead center, which is in the direction of motion of the planet pin and close to the center of pressure between the pin and the planet. The remaining grooves on each planet are located at different azimuthal locations, as indicated in the signal name. At the start of Phase 3 testing, a few of the planet bearing gauges were found to be damaged as described here and annotated in Figure 22 in the Appendix. Signal CD_Kb334_25 was entirely nonfunctional for all Phase 3 testing. Signals AD_Kb00_75 and CU_Kb00_75 were constituted of only the Poisson gauge; signal CD_Kb00_25 was constituted of only the primary gauge.

Thermocouples were also mounted at the axial midpoint of each groove to measure planet bearing inner race temperatures. Two thermocouples (signals AU_Temp0 and BD_Temp0) were not operational as annotated in Figure 22 in the Appendix.

Finally, the inductive proximity sensor intended to sense passage of the 18 rivets in the roller cage of planet A (signal name PlanetA_bearing_slip), was not operational as annotated in Figure 22 in the Appendix. It was removed from the data stream.

4.2.4 Intermediate Stage

Figure 29 in the Appendix shows an updated signal sheet for the intermediate shaft axial position relative to the gearbox housing (signal name ISS_Axial), with the correct sensor type.

4.2.5 High-Speed Shaft

In Phase 3, the HSS instrumentation was significantly enhanced to assess HSS, pinion, and bearing loads. The tapered roller bearing strain gauges were calibrated in a special test rig in May 2013 before being installed in the gearbox [9]. The shaft bending and torque strain gauges were calibrated during the initial HSS installation in November 2013 [6].

Figure 30 in the Appendix shows an updated signal sheet for the HSS encoder. The DAS was configured to calculate the HSS speed (signal name HSS_Speed), from the measured HSS period (signal name HSS_Period). During Phase 3 testing, it was noted that the measured shaft position (signal name HSS_Azimuth), has a 60º offset in it because of the position of the mounting bracket. This offset should be subtracted from all measured HSS_Azimuth values to align with the reference shown in Figure 30 in the Appendix. In this manner, the reference mark on the HSS is pointing up at a value of 0º.

The five proximity sensors that were used to measure the brake disk position relative to the dynamometer floor in Phase 2 (signal names BRK_ appended with direction and position), were not reinstalled for Phase 3 testing. These measurements were deemed to be superseded by the new direct measurements of the HSS loads.

4.3 Lubrication System

The lubrication system is monitored using a variety of sensors. They include the speed of the oil cooler fan (signal name Lube_Fan_Speed); the total flow rate including bypass at the lubrication system pump and flow rate to the gearbox (signal names Lube_Flow_Pump and Lube_Flow_Meter); the pressure at the distribution manifold (signal name Lube_Manifold_Pressure); and the temperatures at the distribution manifold, at the outlet of the oil cooler fan, and at the outlet of the gearbox sump (signal names Lube_Manifold_Temp, Lube_Return_Temp and Sump_Temp).

4.4 Generator

The five proximity sensors that were used to measure generator flange position and rotation relative to the dynamometer floor in Phase 2 (signal names GEN_ appended with direction and position), were not reinstalled for Phase 3 testing. In addition, the encoder on the generator and the resistance temperature detector (RTD) on the downwind generator bearing were not installed.

4.5 Mainframe

The mainframe displacement measurements (signal names FRAME_Z appended with direction), were also not reinstalled for Phase 3 testing.

4.6 Condition Monitoring

The main bearing, gearbox, and lubrication system were also instrumented with various vibration, acoustic emission, and oil analysis condition monitoring systems [10].

4.7 Signal List

The data were recorded in two separate data streams by acquisition rate. A 100-hertz (Hz) rate was used to record information on the planetary and intermediate sections of the gearbox. A 2,000-Hz rate was used to record information on the high-speed section of the gearbox. In each data stream, relevant signals related to the input loading conditions, lubrication system, or output performance of the generator and controller were also recorded. The signals included in each data stream are listed in Table 1 and Table 2, for the 100-Hz and 2,000-Hz rates, respectively. The overwhelming majority of signals were recorded in the engineering units of interest; however, the planetary section and HSS section strain gauges were recorded in native units of millivolts per volt (mV/V). The data files were named beginning with the convention "Test Type_," derived from the name of a particular test in the test plan such as "Static_NTL." "Test Sequence_" follows Test Type and corresponds to sequences in the test plan such as "5A." Finally, the data file names are appended with "YYYY_MM_DD_HH_SS_ZZZZHz.tdms," where YYYY, MM, DD, HH, and SS are the year, month, date, hour, and second of the data acquisition, respectively, and ZZZZ is the acquisition rate in Hertz.

Table 1. Elements of 100-Hz Sample Rate Data

Location	Nomenclature	Expanded Nomenclature	Units	Sensor(s)
DAS	MS Excel Timestamp	Time, MS Excel format, from Jan 1, 1900	days	DAS
DAS	LabVIEW Timestamp	Time, Labview format, from Jan 1, 1904	s	DAS
Dyno	Dyno_Torque	Torque, dynamometer torque spool	kNm	Strain gauge
NTL	NTL_Port_Disp	Displacement, NTL port cylinder	mm	Proximity
NTL	NTL_Port_Force	Force, NTL port cylinder	kN	Load cell
NTL	NTL_Star_Disp	Displacement, NTL starboard cylinder	mm	Proximity
NTL	NTL_Star_Force	Force, NTL starboard cylinder	kN	Load cell
NTL	NTL_Thrust_Disp	Displacement, NTL thrust cylinder	mm	Proximity
NTL	NTL_Thrust_Force	Force, NTL thrust cylinder	kN	Load cell
Main shaft	LSS_TQ	Torque	kNm	Strain gauge
Main shaft	MSBM_YY	Bending moment, rotating, Y-axis	kNm	Strain gauge
Main shaft	MSBM_ZZ	Bending moment, rotating, Z-axis	kNm	Strain gauge
Main shaft	MSBM	Bending moment, total	kNm	Calculated
Main shaft	MSBM_yy	Bending moment, fixed, y-axis	kNm	Calculated
Main shaft	MSBM_zz	Bending moment, fixed, z-axis	kNm	Calculated
Main shaft	LSS_Azimuth	Azimuth angle	deg	Encoder
Main shaft	LSS_Speed	Shaft speed	rpm	Calculated
Housing	Trunion_Z_stbd	Displacement, gearbox Z starboard	mm	Proximity
Housing	Trunion_Z_port	Displacement, gearbox Z port	mm	Proximity
Housing	Trunion_My_bottom	Displacement, gearbox X bottom	mm	Proximity
Housing	Trunion_Y_port	Displacement, gearbox Y port	mm	Proximity
Housing	Trunion_X_stbd	Displacement, gearbox X starboard	mm	Proximity

Location	Nomenclature	Expanded Nomenclature	Units	Sensor(s)
Housing	Trunion_X_port	Displacement, gearbox X port	mm	Proximity
Housing	Case_A_XX	Strain, X, A-location	mV/V	Strain gauge
Housing	Case_A_YY	Strain, Y, A-location	mV/V	Strain gauge
Housing	Case_A_45	Strain, 45°, A-location	mV/V	Strain gauge
Ring gear	Ring_0	Strain, ring gear teeth, 0°, 1st set	mV/V	Strain gauge
Ring gear	Ring_0A	Strain, ring gear teeth, 0°, 2nd set	mV/V	Strain gauge
Ring gear	Ring_120	Strain, ring gear teeth, 120°, 1st set	mV/V	Strain gauge
Ring gear	Ring_120A	Strain, ring gear teeth, 120°, 2nd set	mV/V	Strain gauge
Ring gear	Ring_240_half	Strain, ring gear teeth, 240°, 1st set	mV/V	Strain gauge
Ring gear	Ring_240A	Strain, ring gear teeth, 240° 2nd set	mV/V	Strain gauge
Ring gear	Ring_240_4	Strain, ring gear teeth, 240°, 1st set	mV/V	Strain gauge
Ring gear	EXT_KHB_1	Strain, ring gear tooth, 310°	mV/V	Strain gauge
Ring gear	EXT_KHB_2	Strain, ring gear tooth, 310°	mV/V	Strain gauge
Ring gear	EXT_KHB_3	Strain, ring gear tooth, 310°	mV/V	Strain gauge
Ring gear	EXT_KHB_4	Strain, ring gear tooth, 310°	mV/V	Strain gauge
Ring gear	EXT_KHB_5	Strain, ring gear tooth, 310°	mV/V	Strain gauge
Ring gear	EXT_KHB_6	Strain, ring gear tooth, 310°	mV/V	Strain gauge
Ring gear	EXT_KHB_7	Strain, ring gear tooth, 310°	mV/V	Strain gauge
Ring gear	EXT_KHB_8	Strain, ring gear tooth, 310°	mV/V	Strain gauge
Carrier	Carrier_047	Displacement, carrier, X direction, 047°	mm	Proximity
Carrier	Carrier_137	Displacement, carrier, X direction, 137°	mm	Proximity
Carrier	Carrier_227	Displacement, carrier, X direction, 227°	mm	Proximity
Carrier	Carrier_317	Displacement, carrier, X direction, 317°	mm	Proximity
Carrier	Radial_040	Displacement Radial 40°	mm	Proximity
Carrier	Radial_310	Displacement Radial 310°	mm	Proximity
Planet	PlanetB_Rim_0	Displacement, X direction, 0°	mm	Proximity
Planet	PlanetB_Rim_90	Displacement, X direction, 90°	mm	Proximity
Planet	PlanetB_Rim_180	Displacement, X direction, 180°	mm	Proximity
Planet	PlanetC_Rim_0	Displacement, X direction, 0°	mm	Proximity
Planet	PlanetC_Rim_90	Displacement, X direction, 90°	mm	Proximity
Planet	PlanetC_Rim_180	Displacement, X direction, 180°	mm	Proximity
Planet	AU_Kb00_25	Strain, Planet A, upwind, 0°, 25%	mV/V	Strain gauge
Planet	AU_Kb00_75	Strain, Planet A, upwind, 0°, 75%	mV/V	Strain gauge
Planet	AD_Kb00_25	Strain, Planet A, downwind, 0°, 25%	mV/V	Strain gauge
Planet	AD_Kb00_75	Strain, Planet A, downwind, 0°, 75%	mV/V	Strain gauge

Location	Nomenclature	Expanded Nomenclature	Units	Sensor(s)
Planet	AU_Kb86_25	Strain, Planet A, upwind, 86°, 25%	mV/V	Strain gauge
Planet	AU_Kb86_75	Strain, Planet A, upwind, 86°, 75%	mV/V	Strain gauge
Planet	AD_Kb86_25	Strain, Planet A, downwind, 86°, 25%	mV/V	Strain gauge
Planet	AD_Kb86_75	Strain, Planet A, downwind, 86°, 75%	mV/V	Strain gauge
Planet	AU_Kb274_25	Strain, Planet A, upwind, 274°, 25%	mV/V	Strain gauge
Planet	AU_Kb274_75	Strain, Planet A, upwind, 274°, 75%	mV/V	Strain gauge
Planet	AD_Kb274_25	Strain, Planet A, downwind, 274°, 25%	mV/V	Strain gauge
Planet	AD_Kb274_75	Strain, Planet A, downwind, 274°, 75%	mV/V	Strain gauge
Planet	AU_Temp0	Temperature, Planet A, upwind, 0°	°C	Thermocouple
Planet	AD_Temp86	Temperature, Planet A, downwind, 86°	°C	Thermocouple
Planet	AU_Temp86	Temperature, Planet A, upwind, 86°	°C	Thermocouple
Planet	AD_Temp274	Temperature, Planet A, downwind, 274°	°C	Thermocouple
Planet	PlanetA_OR_temp	Temperature, Planet A, outer race	°C	Thermocouple
Planet	BU_Kb00_25	Strain, Planet B, upwind, 0°, 25%	mV/V	Strain gauge
Planet	BU_Kb00_75	Strain, Planet B, upwind, 0°, 75%	mV/V	Strain gauge
Planet	BD_Kb00_25	Strain, Planet B, downwind, 0°, 25%	mV/V	Strain gauge
Planet	BD_Kb00_75	Strain, Planet B, downwind, 0°, 75%	mV/V	Strain gauge
Planet	BU_Kb256_25	Strain, Planet B, upwind, 256°, 25%	mV/V	Strain gauge
Planet	BU_Kb256_75	Strain, Planet B, upwind, 256°, 75%	mV/V	Strain gauge
Planet	BD_Kb256_25	Strain, Planet B, downwind, 256°, 25%	mV/V	Strain gauge
Planet	BD_Kb256_75	Strain, Planet B, downwind, 256°, 75%	mV/V	Strain gauge
Planet	BU_Kb308_25	Strain, Planet B, upwind, 308°, 25%	mV/V	Strain gauge
Planet	BU_Kb308_75	Strain, Planet B, upwind, 308°, 75%	mV/V	Strain gauge
Planet	BD_Kb308_25	Strain, Planet B, downwind, 308°, 25%	mV/V	Strain gauge
Planet	BD_Kb308_75	Strain, Planet B, downwind, 308°, 75%	mV/V	Strain gauge
Planet	BU_Temp0	Temperature, Planet B, upwind, 0°	°C	Thermocouple
Planet	BD_Temp0	Temperature, Planet B, downwind, 0°	°C	Thermocouple
Planet	BU_Temp256	Temperature, Planet B, upwind, 256°	°C	Thermocouple
Planet	BD_Temp256	Temperature, Planet B, downwind, 256°	°C	Thermocouple
Planet	CU_Kb00_25	Strain, Planet C, upwind, 0°, 25%	mV/V	Strain gauge
Planet	CU_Kb00_75	Strain, Planet C, upwind, 0°, 75%	mV/V	Strain gauge
Planet	CD_Kb00_25	Strain, Planet C, downwind, 0°, 25%	mV/V	Strain gauge
Planet	CD_Kb00_75	Strain, Planet C, downwind, 0°, 75%	mV/V	Strain gauge
Planet	CU_Kb290_25	Strain, Planet C, upwind, 290°, 25%	mV/V	Strain gauge
Planet	CU_Kb290_75	Strain, Planet C, upwind, 290°, 75%	mV/V	Strain gauge

Location	Nomenclature	Expanded Nomenclature	Units	Sensor(s)
Planet	CD_Kb290_25	Strain, Planet C, downwind, 290°, 25%	mV/V	Strain gauge
Planet	CD_Kb290_75	Strain, Planet C, downwind, 290°, 75%	mV/V	Strain gauge
Planet	CU_Kb334_25	Strain, Planet C, upwind, 334°, 25%	mV/V	Strain gauge
Planet	CU_Kb334_75	Strain, Planet C, upwind, 334°, 75%	mV/V	Strain gauge
Planet	CD_Kb334_25	Strain, Planet C, downwind, 334°, 25%	mV/V	Strain gauge
Planet	CD_Kb334_75	Strain, Planet C, downwind, 334°, 75%	mV/V	Strain gauge
Planet	CU_Temp0	Temperature, Planet C, upwind, 0°	°C	Thermocouple
Planet	CD_Temp0	Temperature, Planet C, downwind, 0°	°C	Thermocouple
Planet	CU_Temp290	Temperature, Planet C, upwind, 290°	°C	Thermocouple
Planet	CD_Temp290	Temperature, Planet C, downwind, 290°	°C	Thermocouple
Sun	Sun_radial_ZZ	Displacement, radial, Z direction	mm	Proximity
Sun	Sun_radial_YY	Displacement, radial, Y direction	mm	Proximity
ISS	ISS_Axial	Displacement, X direction	mm	Proximity
ISS	Temp_ISS_DW_brg	Temperature	°C	IR sensor
HSS	HSS_Speed	Shaft speed	rpm	Calculated
HSS	HSS_Azimuth	Azimuth angle	Deg	Encoder
Lube Sys	Lube_Fan_Speed	Speed, lube system fan	rpm	Fan speed
Lube Sys	Lube_Flow_Pump	Flow rate, total, at lube pump	LPM	Fan speed
Lube Sys	Lube_Manifold_Pressure	Pressure, oil at distribution manifold	PSI	Pressure
Lube Sys	Lube_Flow_Meter	Flow rate, to gearbox, at lube pump	LPM	Flow meter
Lube Sys	Lube_Manifold_Temp	Temperature, oil at distribution manifold	°C	RTD
Lube Sys	Lube_Return_Temp	Temperature, oil at cooler fan outlet	°C	RTD
Lube Sys	Sump_Temp	Temperature, oil in gearbox sump	°C	RTD
Controller	Controller_G_contactor	Large generator contactor	-	Relay
Controller	Controller_g_contactor	Small generator contactor	-	Relay
Controller	Controller_bypass_contactor	Soft-start bypass contactor	-	Relay
Controller	kW	Power, real	kW	Transformer
Controller	kVAR	Power, reactive	kVAR	Transformer

13

Table 2. Elements of 2,000-Hz Sample Rate Data

Location	Nomenclature	Expanded Nomenclature	Units	Sensor(s)
DAS	MS Excel Timestamp	Time, MS Excel format, from Jan 1, 1900	days	DAS
DAS	LabVIEW Timestamp	Time, Labview format, from Jan 1, 1904	s	DAS
Dyno	Dyno_Torque	Torque, dynamometer torque spool	kNm	Strain gauge
Main shaft	LSS_TQ	Torque	kNm	Strain gauge
Main shaft	MSBM_YY	Bending moment, Y-axis	kNm	Strain gauge
Main shaft	MSBM_ZZ	Bending moment, Z-axis	kNm	Strain gauge
Main shaft	MSBM	Bending moment	kNm	Calculated
Main shaft	MSBM_yy	Bending moment, fixed, y-axis	kNm	Calculated
Main shaft	MSBM_zz	Bending moment, fixed, z-axis	kNm	Calculated
Main shaft	LSS_Azimuth	Azimuth angle	deg	Encoder
Main shaft	LSS_Speed	Shaft speed	rpm	Calculated
HSS	HSS_UY_BM	Bending, upwind of mesh, YY	mV/V	Strain gauge
HSS	HSS_UZ_BM	Bending, upwind of mesh, ZZ	mV/V	Strain gauge
HSS	HSS_DY_BM	Bending, downwind of mesh, YY	mV/V	Strain gauge
HSS	HSS_DZ_BM	Bending, downwind of mesh, ZZ	mV/V	Strain gauge
HSS	HSS_exY_BM	Bending, External, YY	mV/V	Strain gauge
HSS	HSS_exZ_BM	Bending, External, ZZ	mV/V	Strain gauge
HSS	HSS_TQ	Torque	mV/V	Strain gauge
HSS	TRB_Up_00_A	Strain, upwind TRB, 0°, thin end	mV/V	Strain gauge
HSS	TRB_Up_00_B	Strain, upwind TRB, 0°, thick end	mV/V	Strain gauge
HSS	TRB_Up_90_A	Strain, upwind TRB, 90°, thin end	mV/V	Strain gauge
HSS	TRB_Up_90_B	Strain, upwind TRB, 90°, thick end	mV/V	Strain gauge
HSS	TRB_Up_180_A	Strain, upwind TRB, 180°, thin end	mV/V	Strain gauge
HSS	TRB_Up_180_B	Strain, upwind TRB, 180°, thick end	mV/V	Strain gauge
HSS	TRB_Up_270_A	Strain, upwind TRB, 270°, thin end	mV/V	Strain gauge
HSS	TRB_Up_270_B	Strain, upwind TRB, 270°, thick end	mV/V	Strain gauge
HSS	TRB_Dwn_00_D	Strain, downwind TRB, 0°, thin end	mV/V	Strain gauge
HSS	TRB_Dwn_00_C	Strain, downwind TRB, 0°, thick end	mV/V	Strain gauge
HSS	TRB_Dwn_90_D	Strain, downwind TRB, 90°, thin end	mV/V	Strain gauge
HSS	TRB_Dwn_90_C	Strain, downwind TRB, 90°, thick end	mV/V	Strain gauge
HSS	TRB_Dwn_180_D	Strain, downwind TRB, 180°, thin end	mV/V	Strain gauge
HSS	TRB_Dwn_180_C	Strain, downwind TRB, 180°, thick end	mV/V	Strain gauge
HSS	TRB_Dwn_270_D	Strain, downwind TRB, 270°, thin end	mV/V	Strain gauge
HSS	TRB_Dwn_270_C	Strain, downwind TRB, 270°, thick end	mV/V	Strain gauge

Location	Nomenclature	Expanded Nomenclature	Units	Sensor(s)
HSS	TEMP_TRB_Up	Temperature, upwind TRB	°C	RTD
HSS	TEMP_TRB_Dwn	Temperature, downwind TRB	°C	RTD
HSS	HSP_K1234	Strain, HSS pinion teeth, 1st set	mV/V	Strain gauge
HSS	HSP_Kabcd	Strain, HSS pinion teeth, 2nd set	mV/V	Strain gauge
HSS	HSS_Speed	Shaft speed	rpm	Calculated
HSS	HSS_Azimuth	Azimuth angle	deg	Encoder
Controller	Controller_G_ contactor	Large generator contactor	-	Relay
Controller	Controller_g_ contactor	Small generator contactor	-	Relay
Controller	Controller_bypass_ contactor	Soft-start bypass contactor	-	Relay
Controller	kW	Power, real	kW	Transformer
Controller	kVAR	Power, reactive	kVAR	Transformer

5 Test Sequence

Testing of GB2 in Phase 3 consisted of the following major activities:

- Drivetrain recommissioning
- NTL tests
- HSS radial misalignment tests
- Field representative tests
- Variable speed tests.

5.1 Drivetrain Recommissioning

Recommissioning of the GRC drivetrain began on December 20, 2013. It had not been operated for several years and the HSS signals were newly added and required verification. The tests verified that the drivetrain was operating normally and that all controls and data systems were performing as desired. The recommissioning tests were used to gradually increase speed, torque, and NTLs, with frequent checks to ensure acceptable control and data acquisition performance. These tests lasted until December 27, 2013. The overwhelming majority of data channels were operating properly, except as noted in Section 4.

5.1.1 High-Speed Shaft Investigations

5.1.1.1 High-Speed Shaft Acquisition Rate

As part of the signal verification procedure, the effect of data acquisition rate on the quality of the HSS signals was examined. The maximum acquisition rate that the DAS can record simultaneous data across the multiple backplanes used for GRC instrumentation is just above 2 kHz. Above this, manual disconnection and reconnection of EtherCAT backplanes from the DAS would have been required. This, in turn, would have required the shutdown of the dynamometer.

The relevancy of this acquisition rate is specific to the HSS TRB strain gauge signals. The bearing loads are derived from these signals by measuring the strain resulting from the deflection of a grooved area in the outer race of the bearing as each roller passes underneath, in conjunction with the results from a previous calibration test [9]. During this calibration test, the bearing was rotated by hand approximately 180º and the roller passage events resulted in a signal roughly sinusoidal in nature. The bearing loads were then related to the peak-to-peak amplitude of this sinusoid. Accurately capturing each of the peaks and valleys in each sinusoid, then, is imperative to this process.

At full speed the HSS is rotating at 30 Hz, or 1,800 rpm. In conjunction with the properties of the 32222 J2 TRB, this results in an outer race roller passage frequency of 254.7 Hz. During initial tests, it was noted that the resulting TRB signals had a sawtooth shape, generating concern about properly capturing the peaks and valleys. In this study, HSS data were acquired at the limits of the DAS described earlier, 2 kHz and 5 kHz, equating to an average of 7.8 and 19.6 points per waveform. The data were acquired at power levels of 25%, 50%, 75%, and 100% for 1 s. This resulted in the capture of 254 waveforms, more than enough for determining the loads in steady-state conditions (as long as the peaks and valleys are accurately captured). The NTL system was used to set the main shaft bending moments to near zero. The test was performed on March 13, 2014.

Figure 7 shows an example of the TRB_Up_00_A strain gauge signal for one revolution of the HSS at the 100% power setting. On average, in one revolution of the HSS, 8.5 peaks and valleys are expected. Each signal displays that behavior. In addition, in each signal the valleys are much sharper than the peaks as described earlier. The influence of the HSS bending moment on each signal is also clear, resulting in a once per revolution fluctuation in the signal.
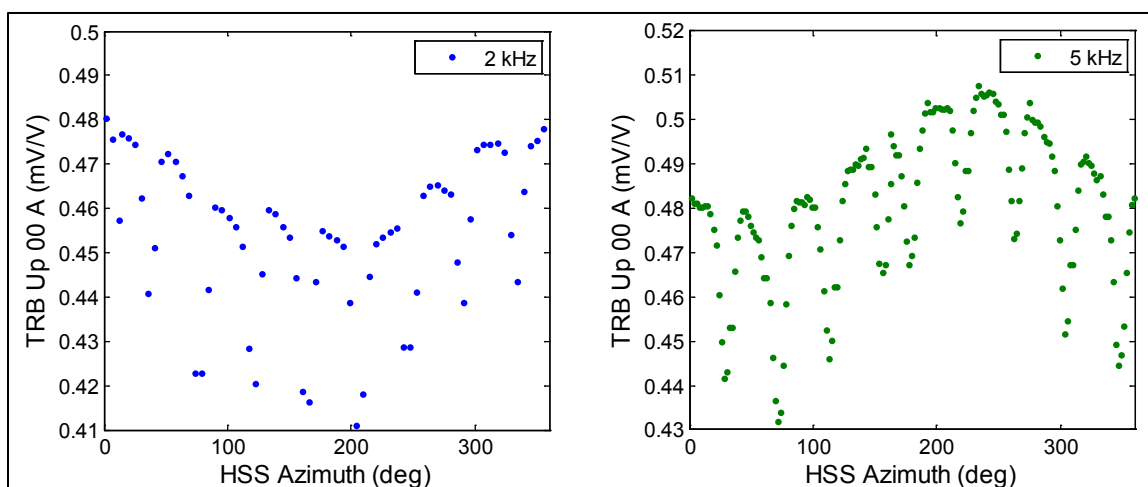

Figure 7. Time domain HSS TRB data

Picking the peaks and valleys in the signal is made more difficult by this bending moment variation. For this reason, the best basis of comparison in the two signals is achieved by transforming them into the frequency domain and examining the signal amplitude at the outer race roller passage frequency as shown in Figure 8. Each acquisition contains strong HSS once-per-revolution content at 30 Hz and outer race roller passage content. At the HSS once-per-revolution frequency, the signals are within 6% of each other; at the outer race roller passage frequency they are within 14% of each other. Although the utmost accuracy is desired for the bearing loads for the purposes of Phase 3 testing the changes in bearing loads between test conditions are more important. For example, when the generator is misaligned, by how much do the bearing loads change? Based on these results, the 2-kHz sampling rate for 1 s was determined to be a sufficient sampling technique for all further testing.
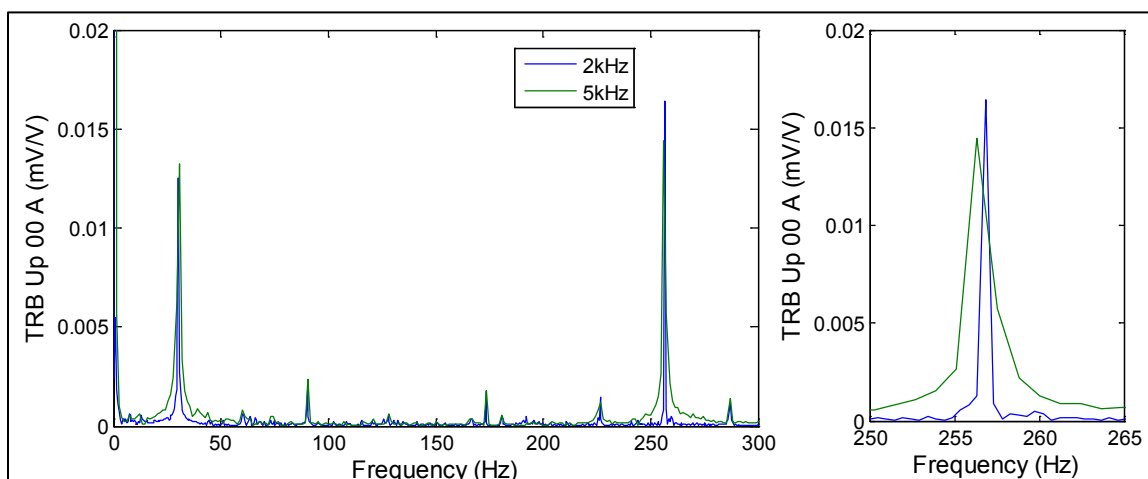

Figure 8. Frequency domain HSS TRB data

17

5.1.1.2 High-Speed Shaft Torque Variation

As noted in the HSS instrumentation calibration report [6], the HSS torque signal varies in magnitude during each rotation of the HSS by as much as 10% of the rated torque. This variation is much larger than expected, and drives a variation in the measured loads of the bearings [11]. This pattern is very consistent from rotation to rotation and is not affected by change in operational torque, even when the generator is offline as shown in Figure 9. In each case, data for 10 revolutions of the HSS are shown. The torque is most consistent at the lower power settings, whereas at power levels of 75% and 100%, the scatter in the data does increase slightly.
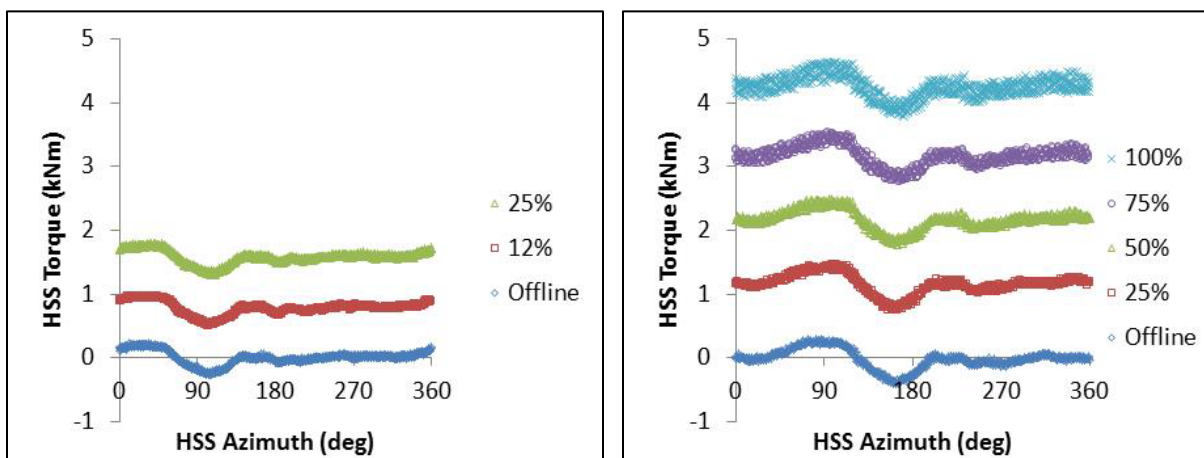
Figure 9. HSS torque data at 1,200 rpm (left) and 1,800 rpm (right)

To investigate this phenomenon, data were acquired at a range of speeds and power settings. Data were acquired on November 20, 2014, in offline conditions at 300, 600, 900, and 1,500 rpm; at 1,200 rpm in offline, 12% power, and 25% power conditions; and at 1,800 rpm in offline, 25% power, 50% power, 75% power, and 100% power conditions. Figure 10 compares the HSS torque in all of the offline conditions. The azimuth and magnitude of the minimum value of torque change with speed. These are lowest and occur at approximately 15º for 300 rpm, 45º for 600 rpm, 75º for 900 rpm, 105º for 1,200 rpm, and 135º for 1,500 rpm. The minimum value of torque is largest at 165º for 1,800 rpm. Several causes for this variation in torque have been proposed, but at this time it is not well understood.
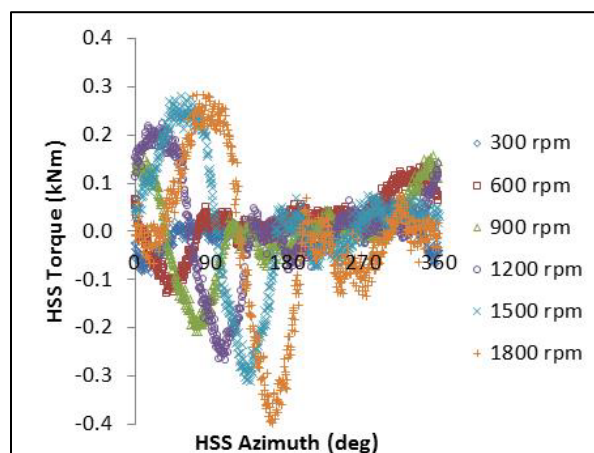

Figure 10. HSS torque data at a range of speeds

18

5.2 Nontorque Load Tests

NTL effects were investigated in Phase 2 tests; however, analysis of test data indicated that the test series was not as comprehensive as desired. In Phase 3 tests, the range of static NTLs was expanded, simple dynamic NTL events were applied, and the response of the gearbox and other drivetrain components were measured more completely.

Immediately after the recommissioning tests, the NTL testing described in the test plan was executed [3]. The NTL tests proceeded from simple static bending moments (gradually increasing in NTL magnitude and power), through simple dynamic bending moments, to static thrust load testing. The following sections describe each test.

5.2.1 Static Bending Moment

The first round of static NTL tests began on December 28, 2013, and lasted until January 3, 2014. The tests were conducted as specified in the test plan, in offline mode (sequences 1–3 and 8) and at 25% power (sequence 4), 50% power (sequence 5), 75% power (sequence 6), and 100% power (sequence 7) conditions. An example of the pitching (M_{yy}) and yawing (M_{zz}) load conditions achieved at 100% power (sequence 7) is shown in Figure 11. The main shaft moments shown have been translated into the fixed frame, using the measured rotating bending moments and azimuth angle. The zero bending moment condition was achieved by operating the drivetrain at full speed, then using the NTL system to apply loads to reduce both measured rotating bending moments to nearly the same value, then using the DAS to zero those values. In other words, the actual main shaft bending moment must be zero when the measured rotating moments are both equal and zeroed. From this point forward, this is called the "taring" and the "tared" condition for the drivetrain. When the drivetrain is tared, the pitching moment caused by the weight of the dynamometer couplings and shafting has been removed from the drivetrain.

In this first round of tests, the yaw moments were limited to ±100 kilonewton-meters (kNm) for all conditions. Above this load, the entire GRC drivetrain yawed slightly and the drivetrain would not return to the same position when unloaded. In this condition, large residual bending moments were measured in the main shaft, affecting the repeatability of test cases.
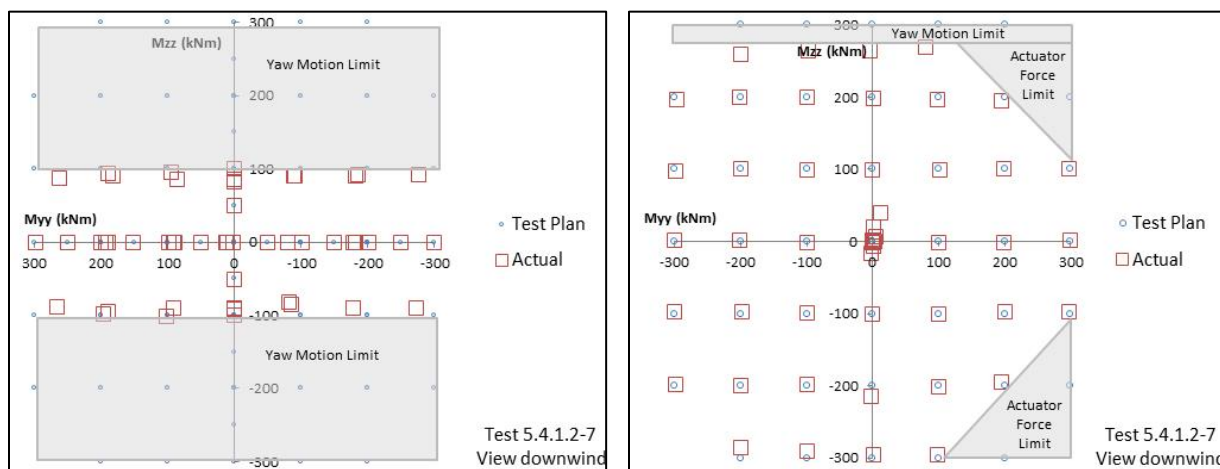

Figure 11. Static NTLs for the first (left) and second (right) tests at 100% power

19

Because of the yaw moment limitations and residual bending moment, the GRC floor adapter plates were redesigned to provide extra clamping force and thereby reduce undesired yaw motion. A new set of plates with a higher factor of safety and provisions for ease of installation was designed and manufactured and then installed in August 2014. Figure 12 is a schematic of the new adapter plates. The second round of static NTL tests was performed from November 11 to 19, 2014. As shown in Figure 11, the new floor adapter plates allowed much larger yaw moments to be reached, and, in some cases, the loading was limited only by the total force provided by each NTL actuator. In the cases in which a residual bending moment was measured (10 to 20 kNm at most), the NTL system was used to re-tare the drivetrain before proceeding to the next test case.
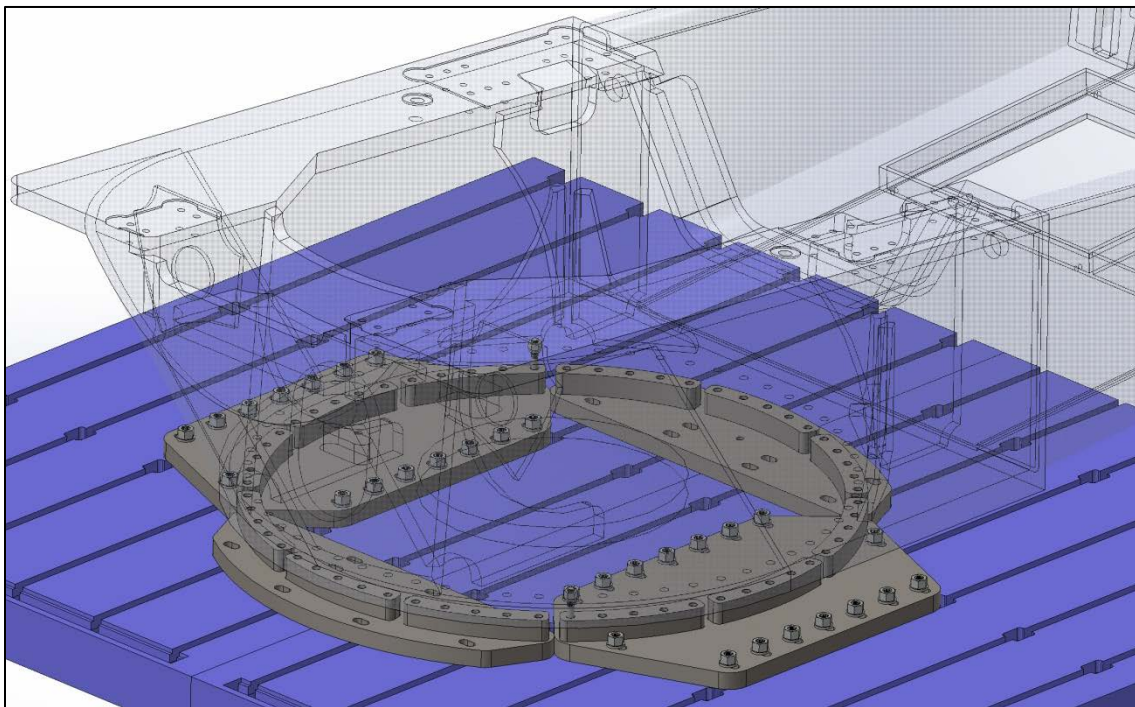

Figure 12. New GRC mainframe-to-dynamometer floor adapter plates. *Illustration by Lambert Engineering*

5.2.2 Dynamic Bending Moment

Dynamic NTL testing was completed on March 18, 2014. Test sequences were completed in offline mode (sequence 1) and at 25% power (sequence 2) and 100% power (sequence 3) conditions with dynamic bending moments at a frequency of 2 Hz as specified in the test plan. Four acquisitions were made for each power setting, representing pitching (M_{yy}) bending moments ranging from 0 to –50 kNm (sequence A) and 0 to –200 kNm (sequence D), and yaw (M_{zz}) moments ranging from 0 to 50 kNm (sequence G) and –100 kNm to 100 kNm (sequence R). Figure 13 shows an example data set for the 100% power, 0- to –50-kNm pitching moment case (sequence 3A). The measured torque is as expected for a full power condition, and the total bending moment on the main shaft ranges between 0 and just under 50 kNm with a frequency of 2 Hz.
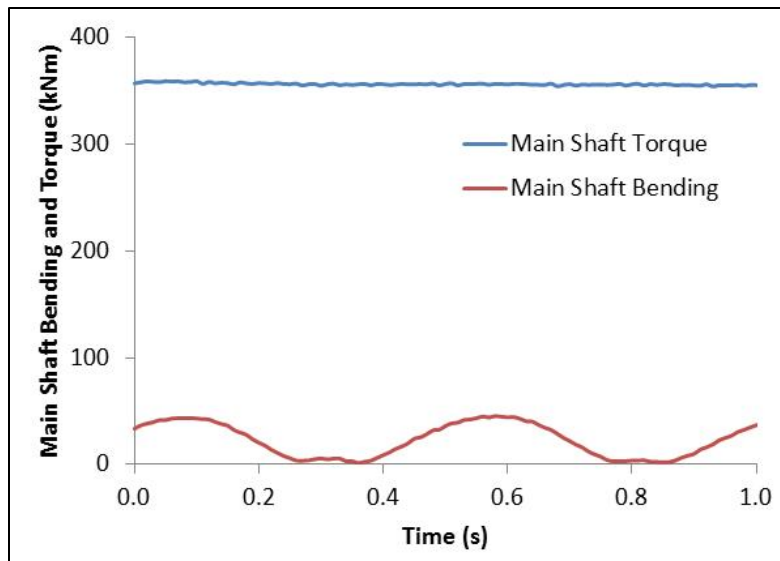
Figure 13. Dynamic NTLs at 100% power

5.2.3 Static Thrust

Static thrust testing was also completed on March 18, 2014. Test sequences were completed in offline mode (sequence 1 and 2) and at 25% power (sequence 3), 50% power (sequence 4), 75% power (sequence 5), and 100% power (sequence 6) conditions as specified in the test plan. For sequences 2 through 6, the NTL system was used so that there was no measured main shaft bending moment. Nine acquisitions were made for each power setting, representing thrust loads (F_z) ranging from –100 to 100 kN in 50-kilonewton (kN) increments.

5.3 Generator Misalignment Tests

In Phase 2, the generator was misaligned. The HSS bearings were instrumented only with temperature sensors, so it was not possible to measure the effect of the misalignment on loads. By outfitting the HSS with instrumentation on the shaft, pinion, and bearings, Phase 3 tests were intended to clarify what conditions, if any, impart excessive loads onto the HSS bearings.

In Phase 3, generator misalignment testing was performed from November 21 to December 30, 2014. The generator was intentionally misaligned from the gearbox by shimming it by the same amount under each of the mounting feet—radially misaligning the generator. Shim stacks of 5.08, 10.95, 21.90, and 32.06 mm resulted in approximate radial misalignment angles of 0.5º, 1º, 2º, and 3º, respectively. It should be noted that the nominal generator alignment was set in a nonoperational state (i.e., with the weight of the dynamometer coupling creating a pitching moment on the gearbox). It should also be noted that the generator coupling does exert some force on the gearbox when the generator is misaligned. Because the gearbox trunnion mounts do have some elastic stiffness, this serves to reduce the misalignment angle slightly.

Data were acquired in offline mode (sequence 1 and 2) and at 25% power (sequence 3), 50% power (sequence 4), 75% power (sequence 5), and 100% power (sequence 6) conditions. In addition, data were acquired in an offline condition at a speed of 1 rpm and when the drivetrain was fully stopped to yield measurements of the gearbox position. In each case, data were acquired with the main shaft in untared conditions. This was because at the 3º misalignment

condition allowed per the coupling specification, the generator coupling links almost touched the brake disk and generator flange. When the drivetrain was tared, the gearbox displaced just enough that the coupling links actually came into contact with the brake disk and flange. This contact was undesirable because it would tend to introduce unwanted vibratory loading into the HSS section. The shim stacks and resulting generator coupling misalignment are shown in Figure 14 for the 3º condition.
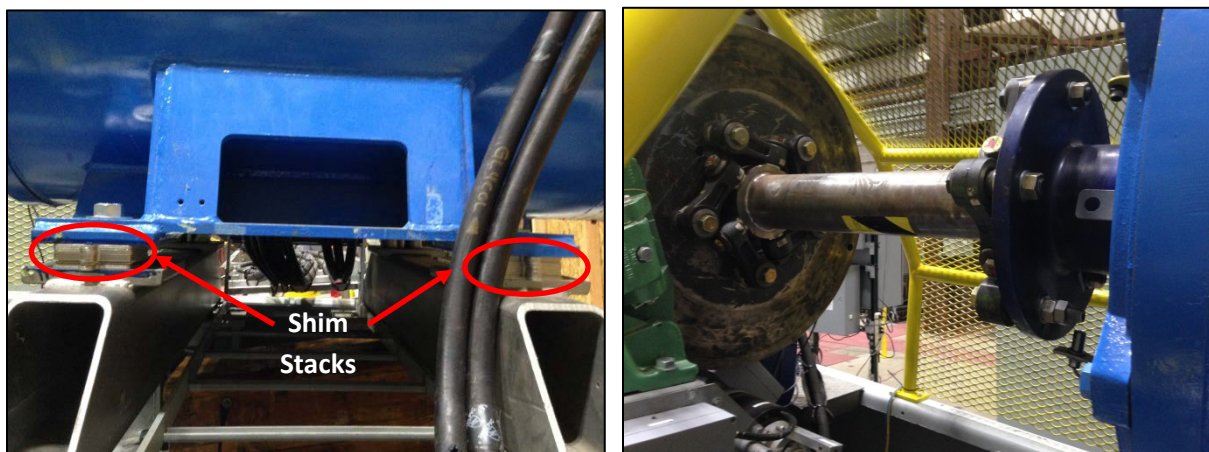

Figure 14. Generator shim stack (left) and generator coupling (right) at 3º misalignment. *Photos by Jon Keller, NREL 32491 and 32492*

Example results for the misalignment tests are shown in Figure 15. The average bending moment measured between the TRB pair and the generator coupling, derived from signals HSS_exY_BM and HSS_exZ_BM, is compared for the range of static generator misalignment angles. The bending moment is substantially reduced by introducing a premisalignment up to 2º. Above that the bending moment increases. This premisalignment actually relieves the bending moment induced by the weight of the brake disk and the coupling itself. The bending moments are a driver of loads within the individual TRBs, so further analysis is required; however, the initial results indicate that premisalignment can reduce loads in HSS bearings.
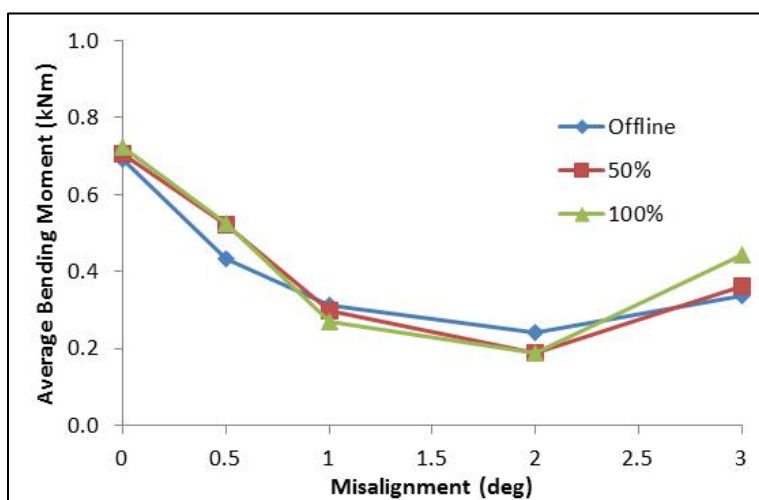

Figure 15. Effect of generator misalignment on measured HSS bending moment

5.4 Field Representative Tests

Approximately 3 months of field testing occurred during the GRC Phase 1. Among many measurements acquired were the main shaft torque and planetary system loads. The HSS torque or the HSS bearing loads were not measured during the field test. Reproduction of field conditions in the dynamometer was attempted in Phase 2 testing; however, a key shortfall in the NWTC 2.5-MW dynamometer at that time was the limited control bandwidth of the VFD.

As described in Section 3.1, NREL replaced the 2.5-MW dynamometer VFD with a modern and more reliable drive before Phase 3 testing. The test sequence described in this section was enabled by that new capability. Examples of field representative testing completed in Phase 3 testing are discussed in the following sections. These examples correspond to normal power production and shutdown cases, respectively.

5.4.1 Normal Power Production

The normal power production case was first attempted in April 2014. After analysis, slight modifications were made to the test process and the test was completed in January 2015. The tests proceeded in a graduated fashion, beginning with the low torque and NTLs for the 5-m/s wind speed case, then increasing them for the 15-m/s case, and increasing them again to near rated values for the 25-m/s case. In each case, a system identification test was performed, in which the desired dynamic torque was commanded and the actual torque was measured. This measured response was then used to tailor the commanded dynamic torque to result in a main shaft torque close to the values measured in the field. In each case, the NTLs were simply operated in force-feedback mode. The test for each wind speed case lasted 11 min, including a 30-s ramp-up period to full loads at the beginning of the test and a 30-s ramp-down period at the end of the test. A 10-s snapshot of the results for the 25-m/s wind speed case is shown in Figure 16. The measured torque and bending moments in the dynamometer show excellent correlation with those measured in the field.
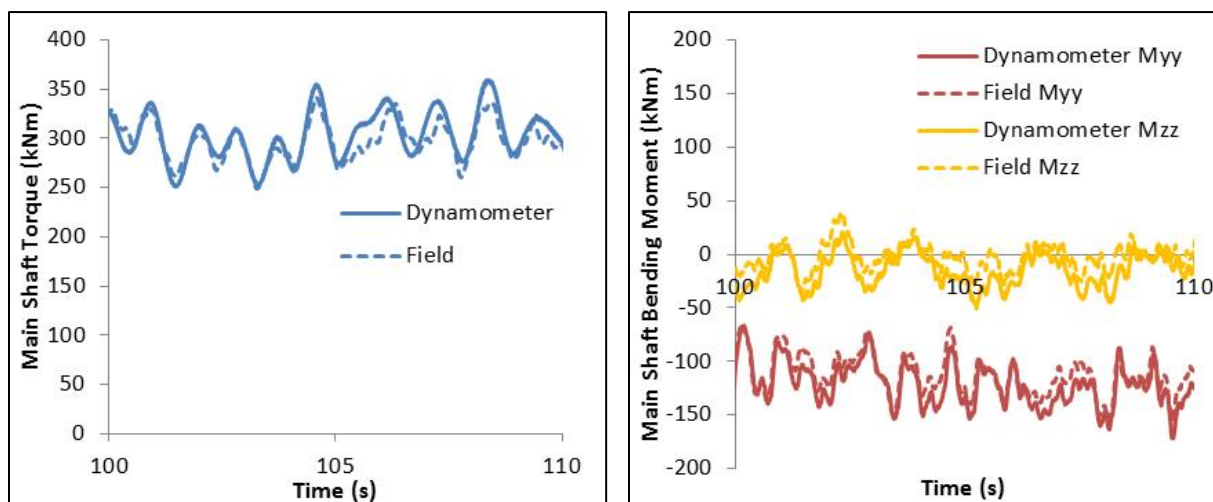

Figure 16. Main shaft torque (left) and bending moments (right) for the 25-m/s wind speed case

5.4.2 Shutdown

The GRC drivetrain uses a SIME-Stromag 3TWa37-TE2L single-caliper disk brake system. It is a fail-safe system with an electrohydraulic release. The brake disk is mounted with an interference fit to the end of the HSS. The braking system hardware is shown in Figure 17.

Figure 17. GRC braking system hardware. *Photo by Joe Verrengia, NREL 16867*

For the shutdown case, the loads reached immediately after engaging the disk brake are of primary interest. The shutdown event measured in the field, from Appendix C of the test plan, is shown in the left portion of Figure 18. The initial portion of the shutdown, in which the controller disconnected the generator from the grid and actuated the rotor tip brakes to slow the rotor, is not shown. The portion shown in Figure 18 is from 1 s before the disk brake application to 9 s after the rotor stops. The maximum torque of just over 160% of rated occurred immediately after the application of the HSS brake at 20 s at approximately 45% rotor speed (10 rpm). The rotor and main shaft take approximately 5 s to come to a full stop. During those seconds, the main shaft torque oscillates through multiple cycles. The main shaft torque continues to oscillate even after the rotor stops for multiple cycles.

The shutdown event in the dynamometer was completed in late December 2014 and again in early January 2015. Each test was completed with the generator offline, so that the initial torque was essentially zero as in the field. The operation of the braking system hardware and software controls was verified in a graduated fashion. The system was programmed to actuate the brake calipers when the dynamometer crossed below a configurable speed. The response of the drivetrain to the actuation speed was examined thoroughly, beginning with a brake application at 1% speed (0.25 rpm), to determine the resulting maximum torque value. The brake application speed was then slowly increased until the field speed was reached, ensuring that the maximum torque did not exceed 200%. The final test, where the torque reached 189% of rated, is shown in the right portion of Figure 18. The maximum torque was very similar to the field value, which was the primary goal of the test. The brake was also able to stop the dynamometer in about 4 s,

which was very similar to the rate at which it stopped the rotor in the field. During this period, however, the main shaft torque measured in the dynamometer did not decay as rapidly as it did in the field, likely because aerodynamic damping is lacking, and does not have the same frequency content as it did in the field because the drivetrain rotational frequencies are different.
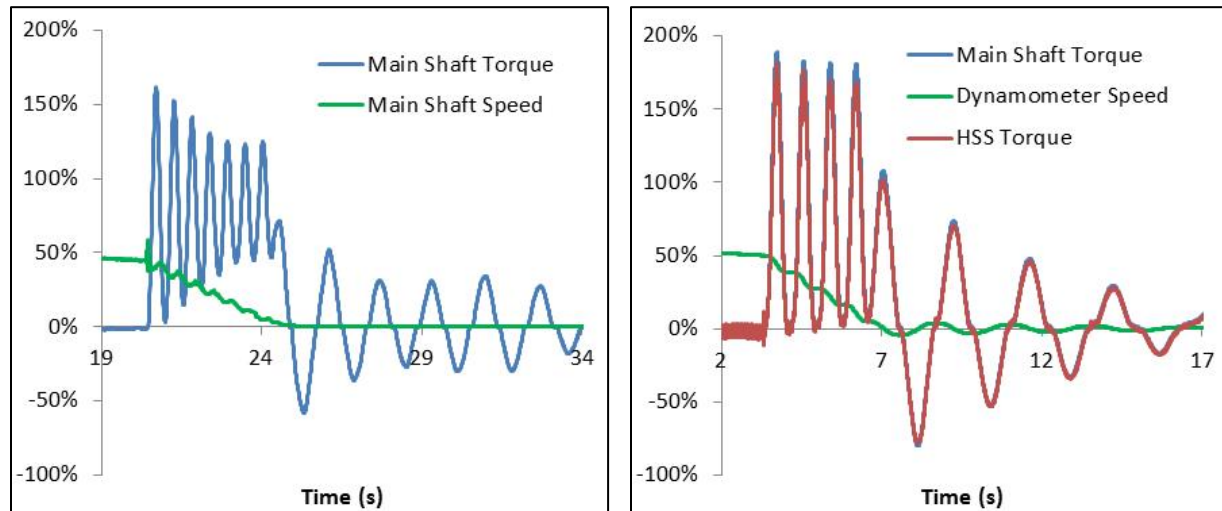

Figure 18. Shutdown event in the field (left) and dynamometer (right)

5.5 Grid Disconnect Tests

The Campbell Diagram test described in the test plan was not performed. Because the GRC drivetrain is a two-speed system, an expensive eddy current brake would have been required to run the drivetrain at variable speeds while under load. It was determined that such a system was beyond the scope of Phase 3 efforts.

Instead, a controlled shutdown was performed. In this test, while operating at a steady-state power level, the dynamometer was intentionally shut down in a controlled fashion. The GRC generator immediately disconnected and the dynamometer ramped down at a controlled speed, taking about 3 min to come to a complete stop. The tests were first partially performed on April 29, 2014, and then completely performed on November 20, 2014. Shutdowns were performed at 25% power, 50% power, 75% power, and 100% power. Example results for the shutdown from 100% power are shown in Figure 19 for only the first 10 s of the event. The main shaft speed data have been de-noised for purposes of illustration; however, what appears to be noise in the HSS torque signal is actually the 10% torque oscillation shown in Figure 9.

At approximately 2 s, the shutdown began. The generator almost immediately disconnected, dropping to no power, and the dynamometer began a slow deceleration from full speed to approximately 85% speed at 10 s. The most interesting behavior was that of the torque data for both the main shaft and the HSS. When the generator was operating at rated power, the HSS was carrying the expected full torque. When the generator was disconnected, the torque quickly dropped and *reversed* to greater than 60% of rated and oscillated for multiple cycles, finally decaying to near zero torque at 10 s.

It should also be noted that the behavior wherein the GRC controller immediately disconnects the generator from the grid is the same behavior the controller would exhibit in response to a grid

event. The slow ramp-down in speed is governed by inertia and damping in the drivetrain and dynamometer (i.e., the system coasts to a stop). Only the initial torque reversal, then, is really representative of the behavior that the drivetrain would exhibit in the field for a grid disconnect event because the damping and inertia differs between the dynamometer and the field.
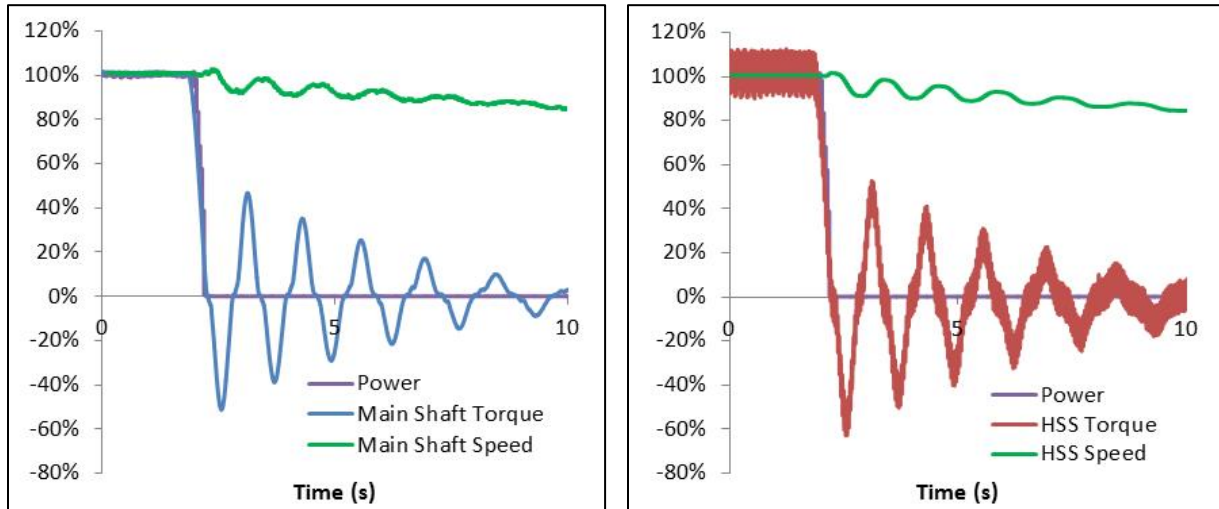

Figure 19. Main shaft (left) and HSS (right) response during controlled dynamometer shutdown

6 Summary

The GRC uses a combined gearbox testing, modeling, and analysis approach to investigate gearbox responses to specified loading conditions. Knowledge gained by comparing publicly available engineering models to measured data is disseminated to the industry, which facilitates gearbox reliability improvements. Ideally, the knowledge gained from the GRC will result in improvements to gearbox design standards and associated modeling tools.

This report describes the recent tests of GRC GB2 in the NWTC 2.5-MW dynamometer conducted during a few periods from December 2013 to early January 2015. Specific objectives of the test were to assess the effect of static and dynamic NTLs on the planetary section, generator misalignment on the HSS section, and field representative conditions on the gearbox in general. The report serves as a guide for interpreting the publicly available data sets with brief analyses to illustrate the data. The data and engineering details of the gearbox are publicly available [12].

References

1. Sheng, S. (2013). *Report on Wind Turbine Subsystem Reliability—A Survey of Various Databases*. NREL/PR-5000-59111. Golden, CO: NREL.

2. Link, H.; LaCava, W.; van Dam, J.; McNiff, B.; Sheng, S.; Wallen, R.; McDade, M.; Lambert, S.; Butterfield, S.; Oyague, F. (2011). *Gearbox Reliability Collaborative Project Report: Findings from Phase 1 and Phase 2 Testing*. NREL/TP-5000-51885. Golden, CO: NREL.

3. Link, H.; Keller, J.; Guo, Y.; McNiff, B. (2013). *Gearbox Reliability Collaborative Phase 3 Gearbox 2 Test Plan*. NREL/TP-5000-58190. Golden, CO: NREL.

4. Scott, K.G.; Infield, D.; Barltrop, N.; Coultate, J.K.; Shahaj, A. (2012). "Effects of Extreme and Transient Loads on Wind Turbine Drive Trains." 50th AIAA Aerospace Sciences Meeting Including the New Horizons Forum and Aerospace Exposition. Reston, VA: The American Institute of Aeronautics and Astronautics. doi: 10.2514/6.2012-1293.

5. Jain, S.; Hunt, H.E.M. (2011). "A Dynamic Model to Predict the Occurrence of Skidding in Wind-Turbine Bearings." *Journal of Physics: Conference Series 305*. Philadelphia, PA: IOP Publishing. doi:10.1088/1742-6596/305/1/012027.

6. Keller, J.; McNiff, B. (2014). *Gearbox Reliability Collaborative High Speed Shaft Calibration*. NREL/TP-5000-62373. Golden, CO: NREL.

7. "Dynamometer Testing." (2010). NREL/FS-5000-45649. Golden, CO: NREL, Accessed November 20, 2012: http://www.nrel.gov/docs/fy11osti/45649.pdf.

8. ACS2000 (Medium Voltage AC Drive). "Flexible and Reliable: Technology Leading Medium Voltage Drives for a Wide Variety of Applications." Zurich, Switzerland: ABB. Accessed February 12, 2015: http://new.abb.com/drives/medium-voltage-ac-drives/acs2000.

9. Keller, J.; Guo, Y.; McNiff, B. (2013). *Gearbox Reliability Collaborative High Speed Shaft Tapered Roller Bearing Calibration*. NREL/TP-5000-60319. Golden, CO: NREL.

10. Sheng, S.; Wallen, R. (2014). *Wind Turbine Gearbox Condition Monitoring Based on GRC Phase 3 Gearbox 2 Testing*. NREL/TP-5000-61748. Golden, CO: NREL.

11. McNiff, B.; Guo, Y.; Keller, J.; Sethuraman, L. (2014). *High-Speed Shaft Bearing Loads Testing and Modeling in the NREL Gearbox Reliability Collaborative: Preprint*. NREL/CP-5000-63277. Golden, CO: NREL.

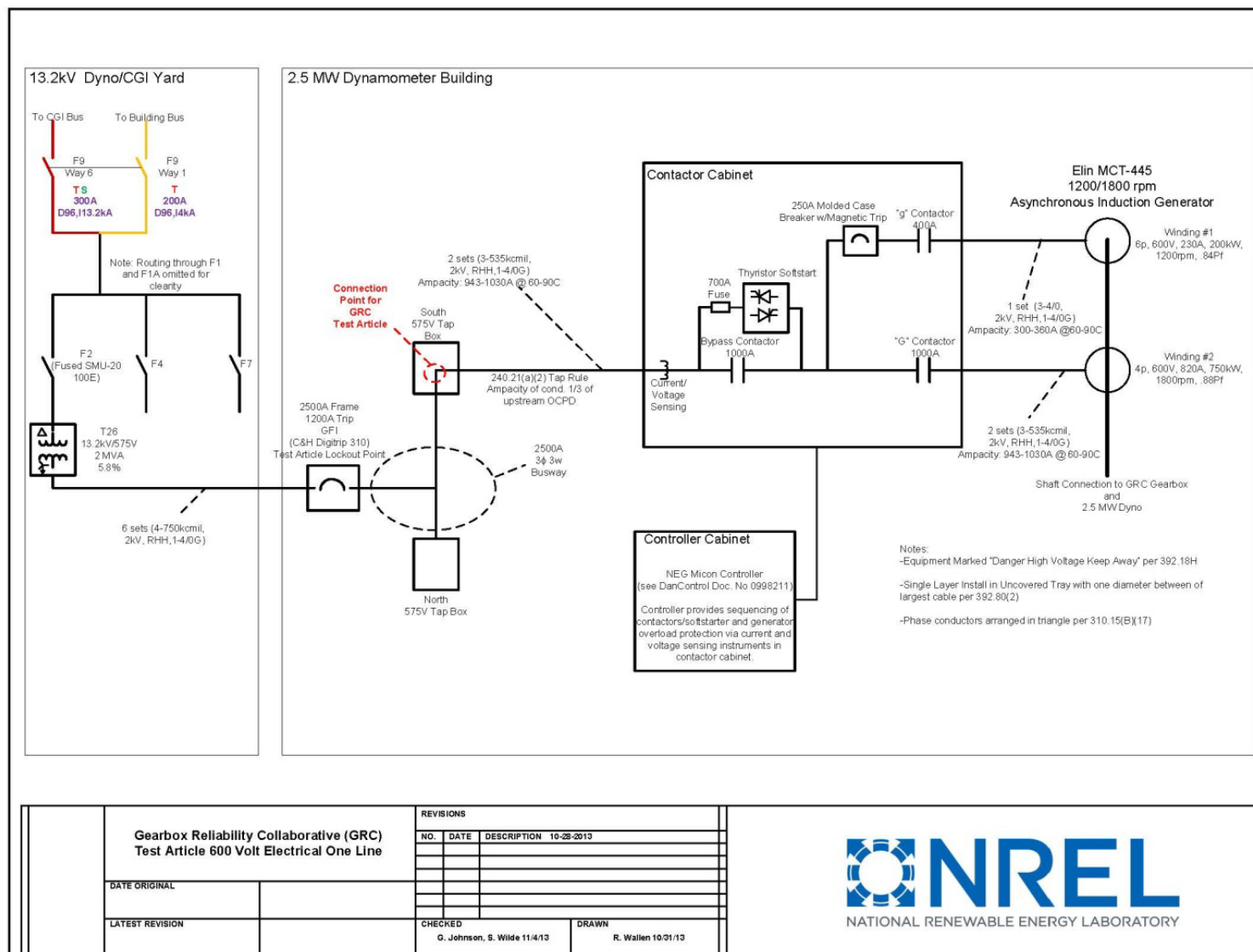12. NREL Data Catalog. "Gearbox Reliability Collaborative Phase 3 Gearbox 2 Test." https://doi.org/10.7799/1254154.

Appendix

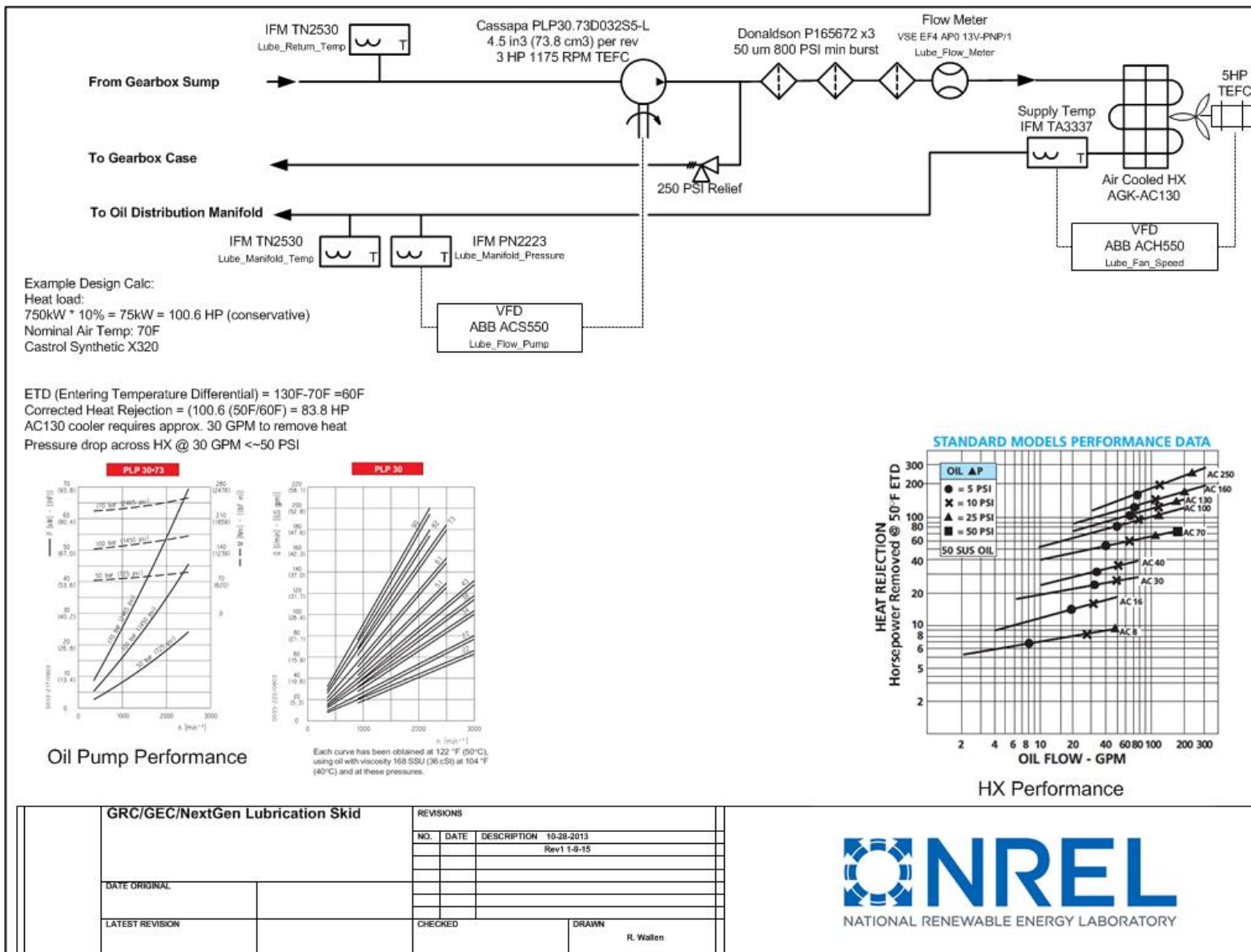**Figure 20. GRC electrical interconnection**

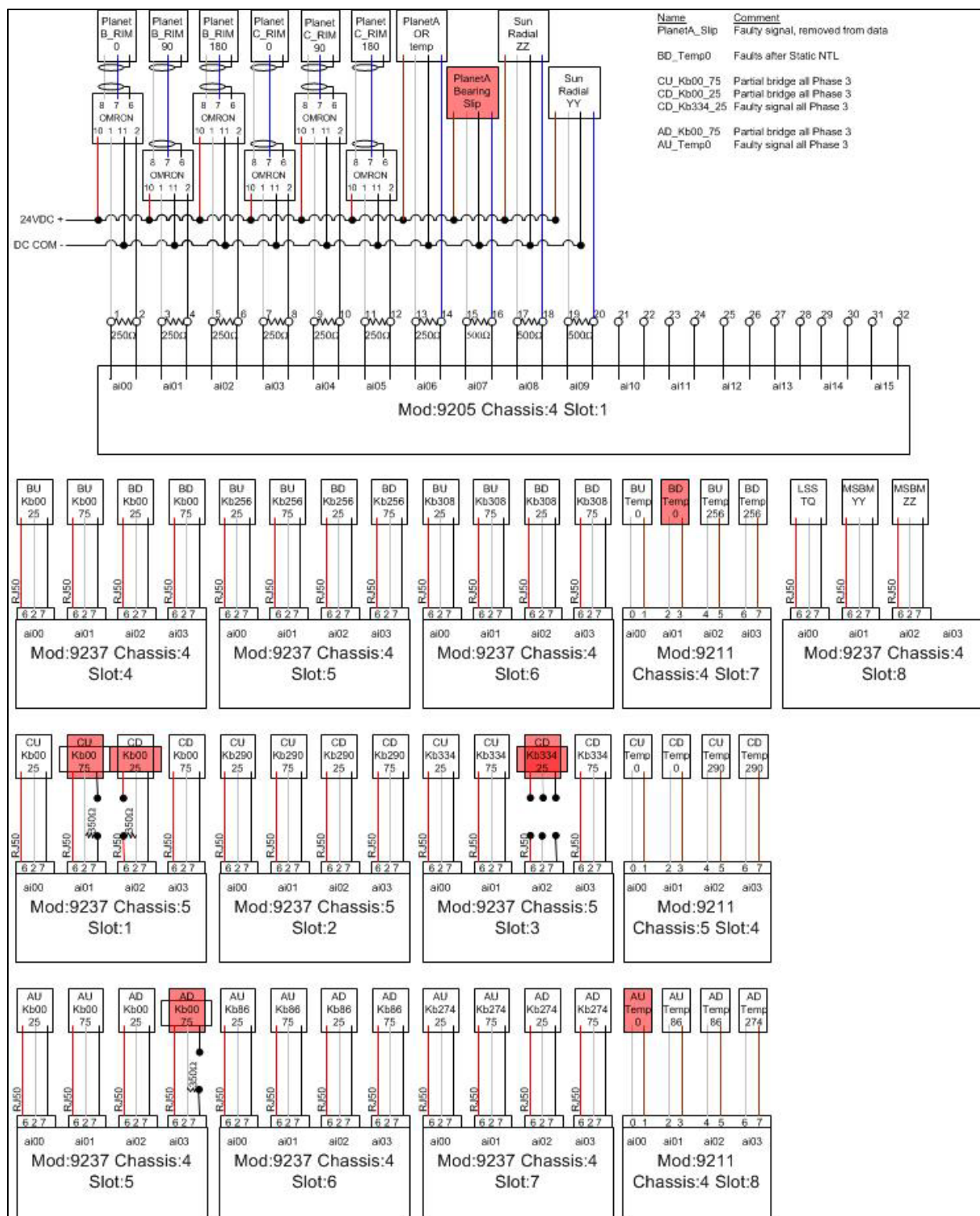**Figure 21. Lubrication system schematic**

Figure 22. LSS DAS box configuration

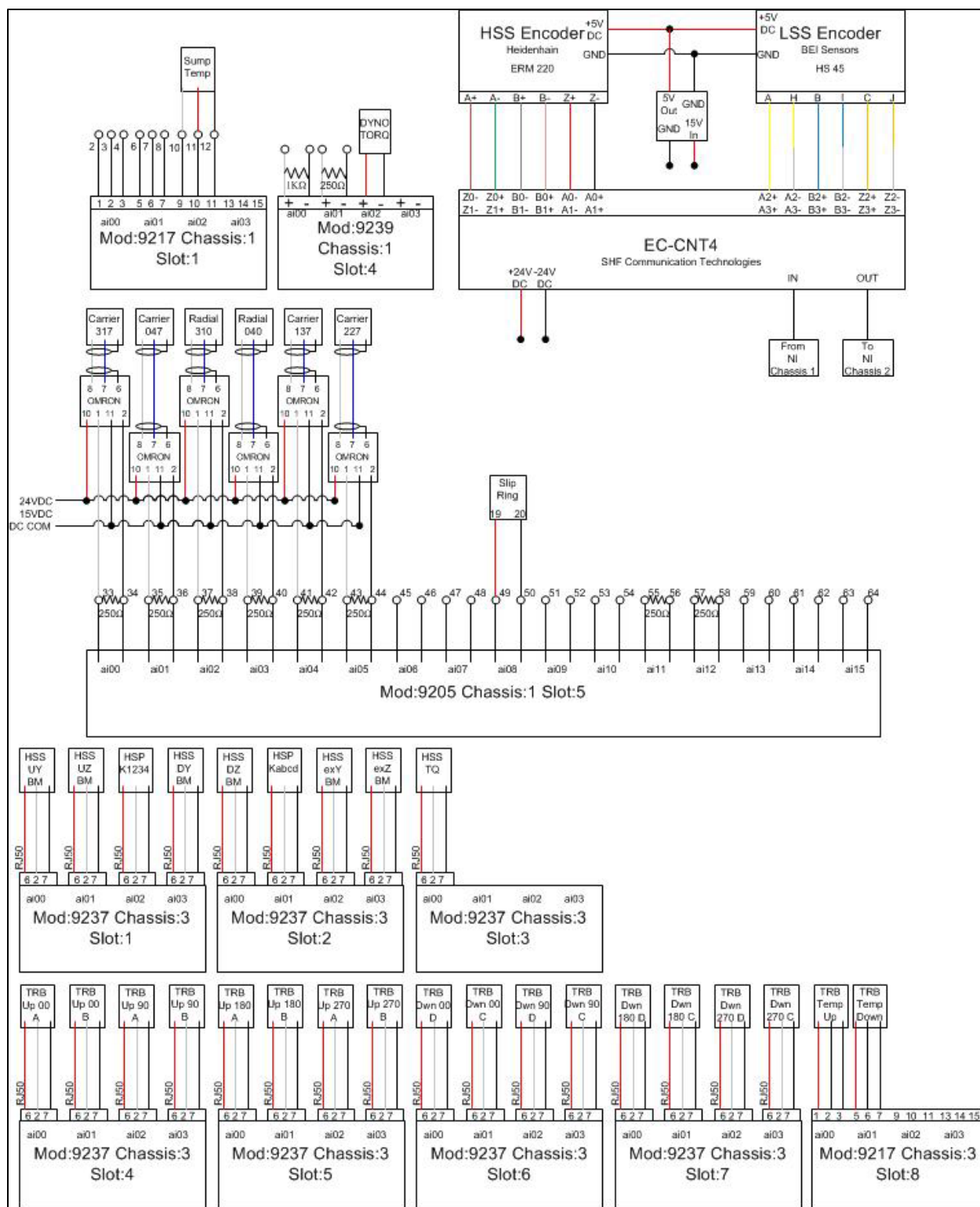**Figure 23. Port DAS box configuration**
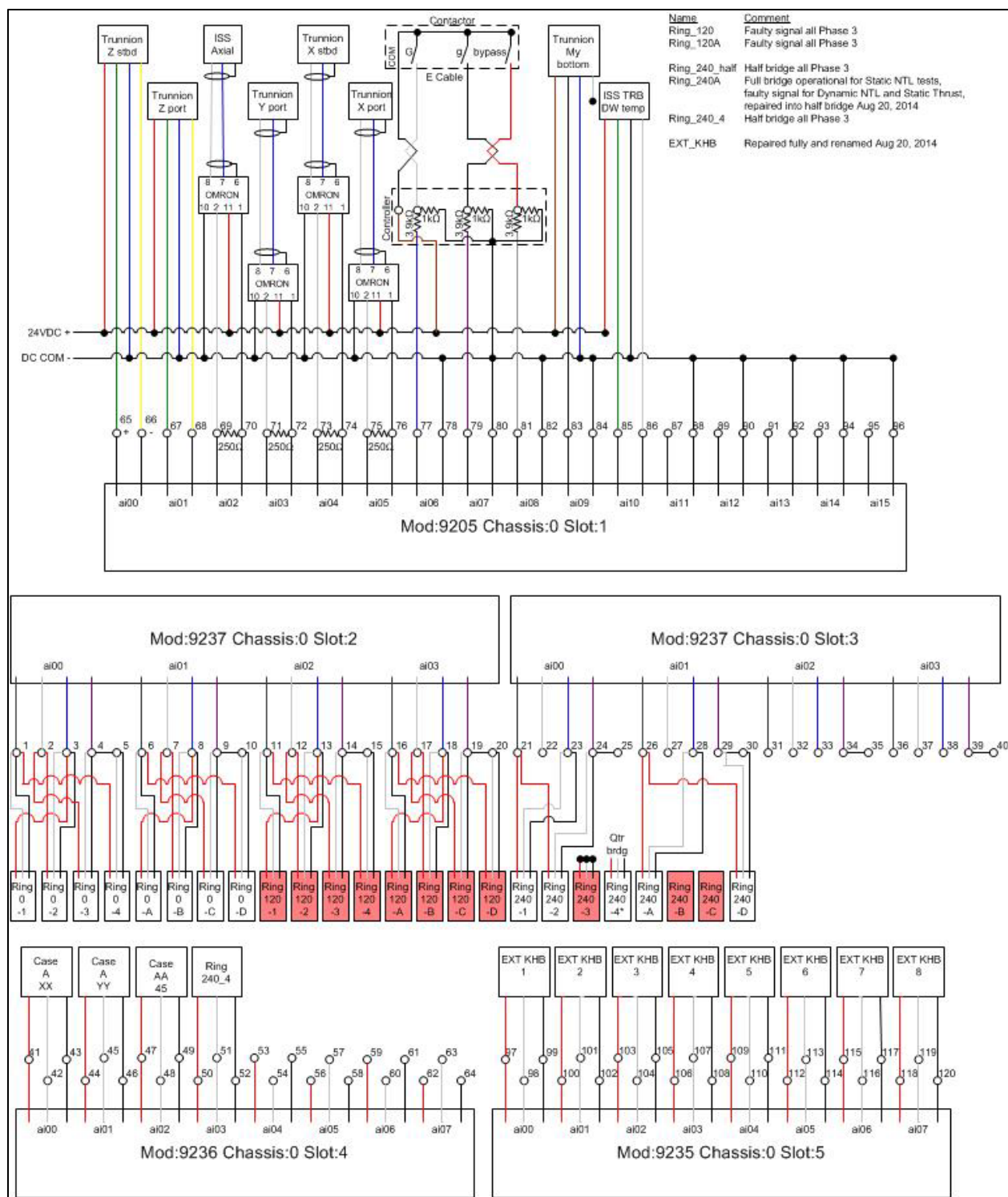
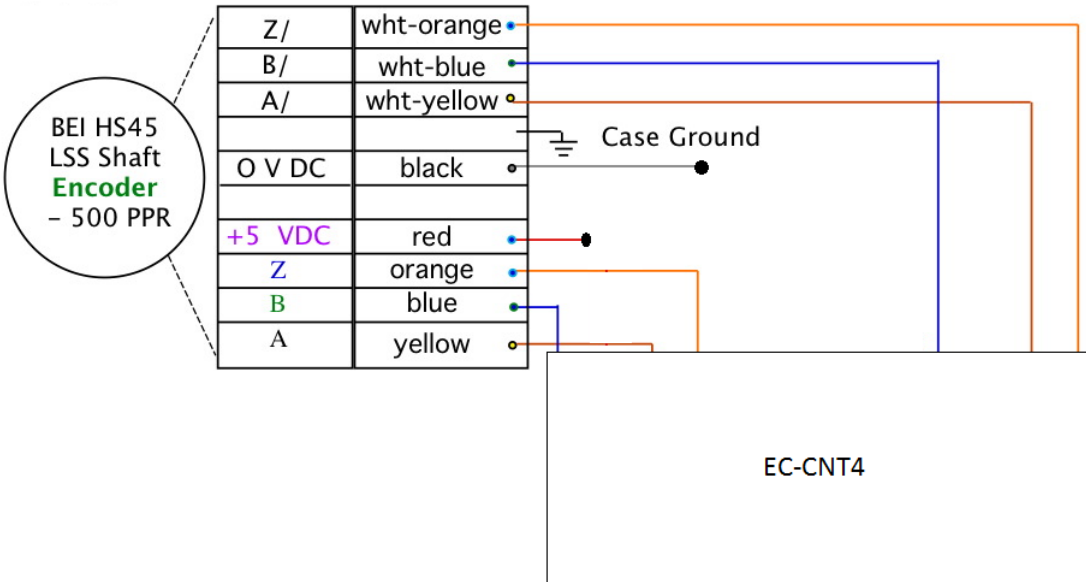**Figure 24. Starboard DAS box configuration**

Figure 25. Main shaft speed and azimuth
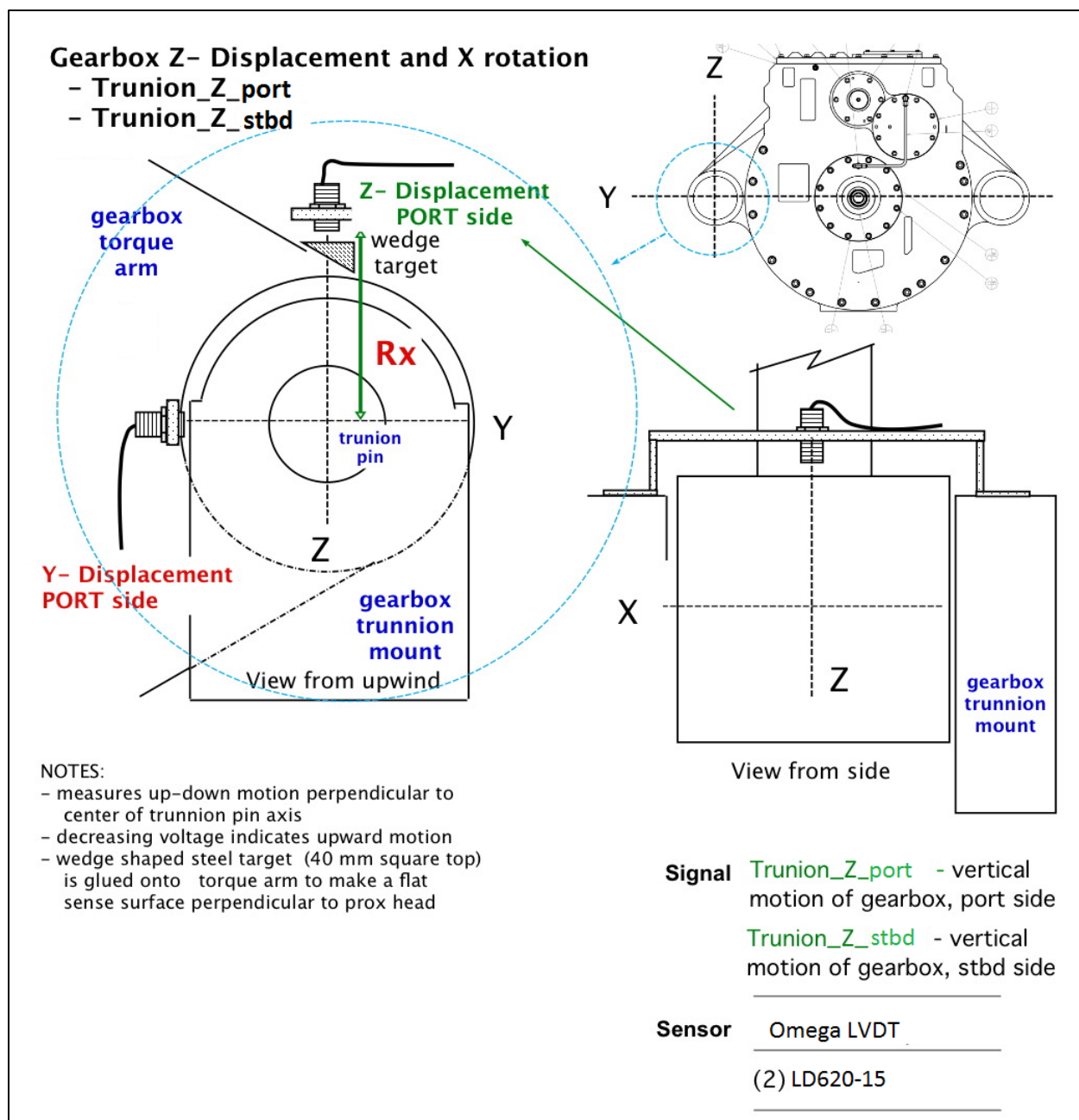
Figure 26. Gearbox motion, ZZ, at trunnion

Gearbox Rotation about Y-axis
– Trunion_My_bottom

Z

X

SEE DETAIL A

J

R ~ 2 inches

locate
to target
center of
gearbox

~4 inches

Cross beam
on nacelle frame
below gearbox

set to 8 mm gap

Notes on sensor mount:
– top hole – M18 thread
– bottom holes (2) allow for
   for 1/4–20 screws

SIGNAL	**Trunion_My_bottom**
SENSOR	Eaton Accurprox
	E59-A18A107C02-CV

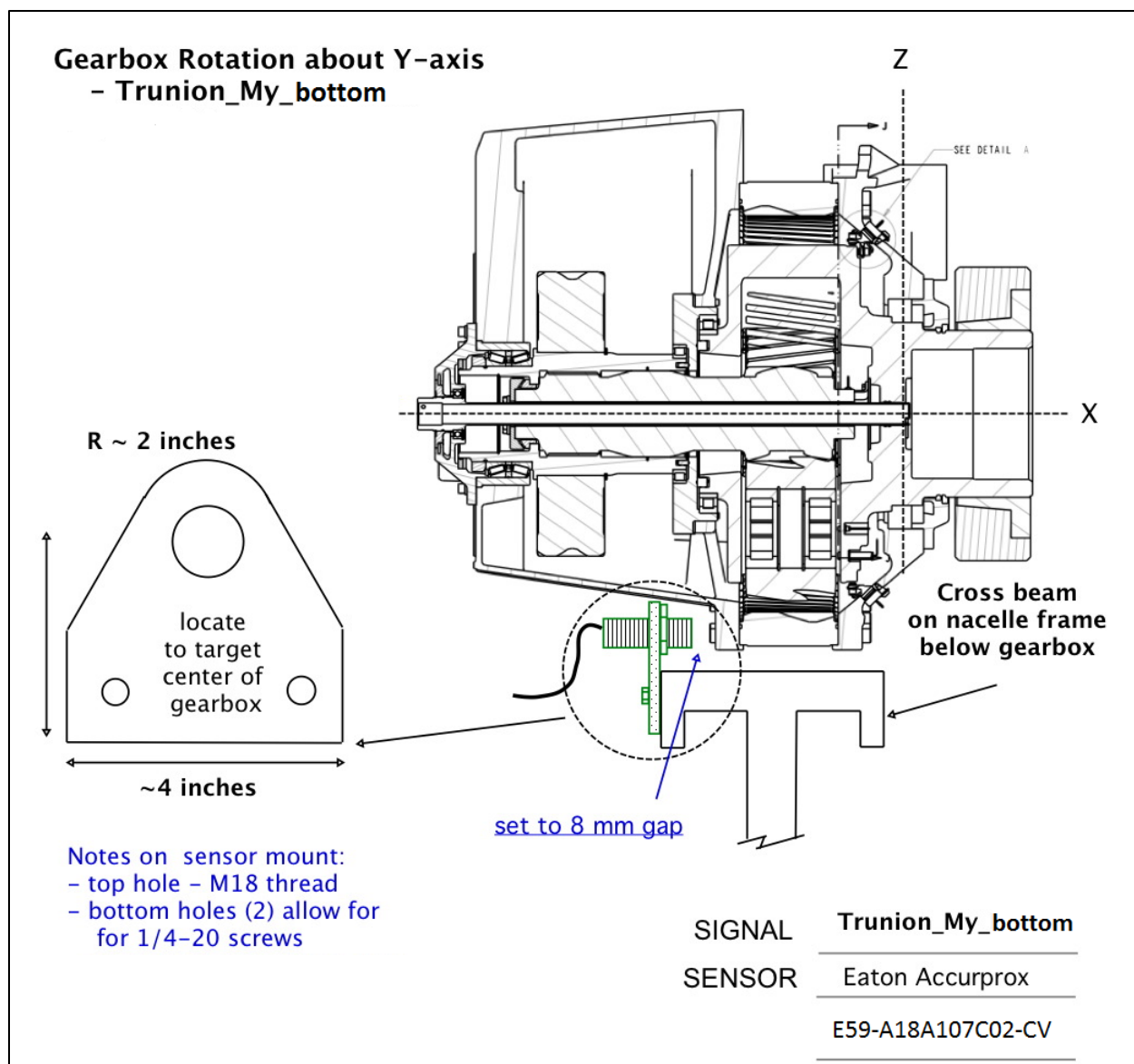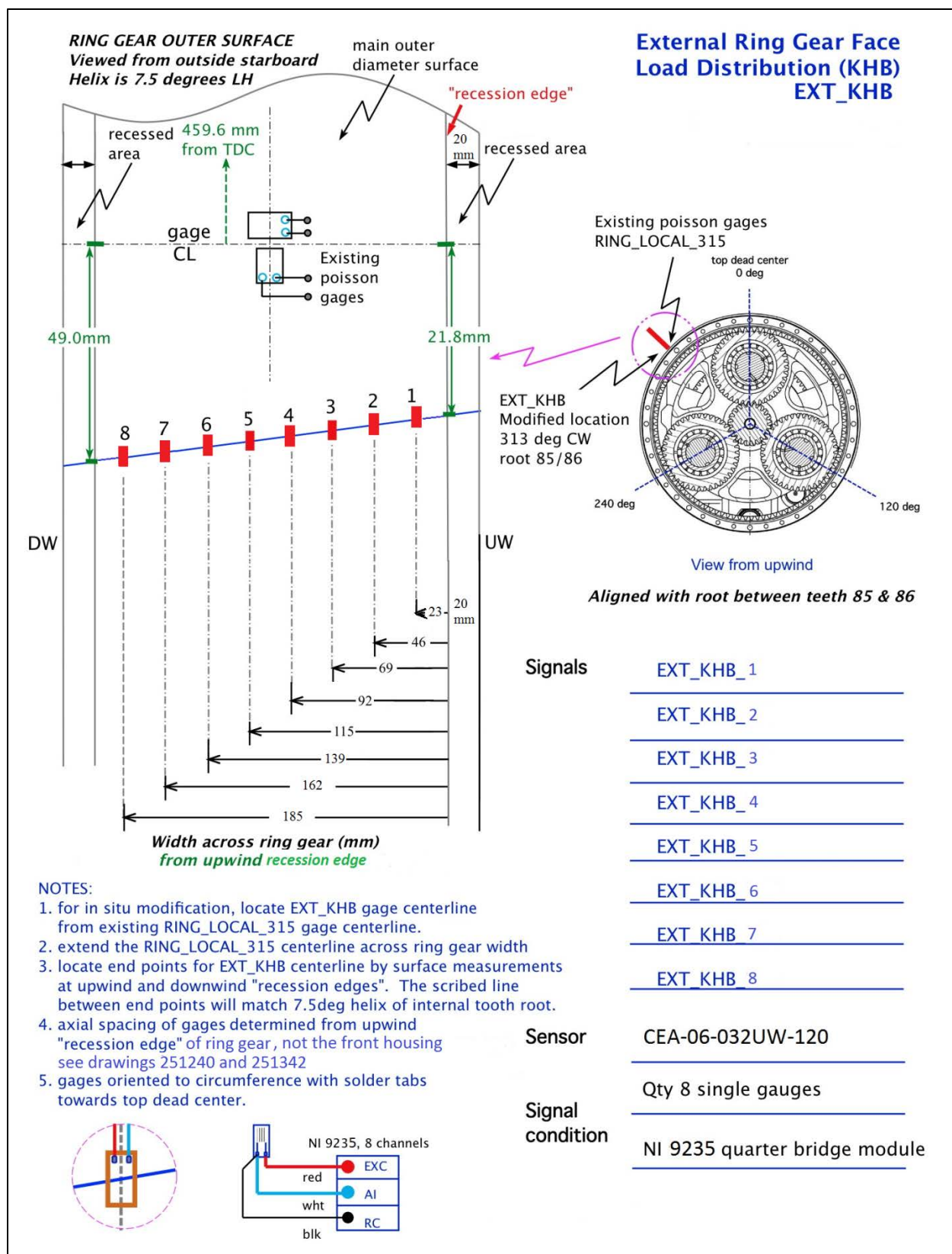**Figure 27. Gearbox motion, YY, bottom rotation**

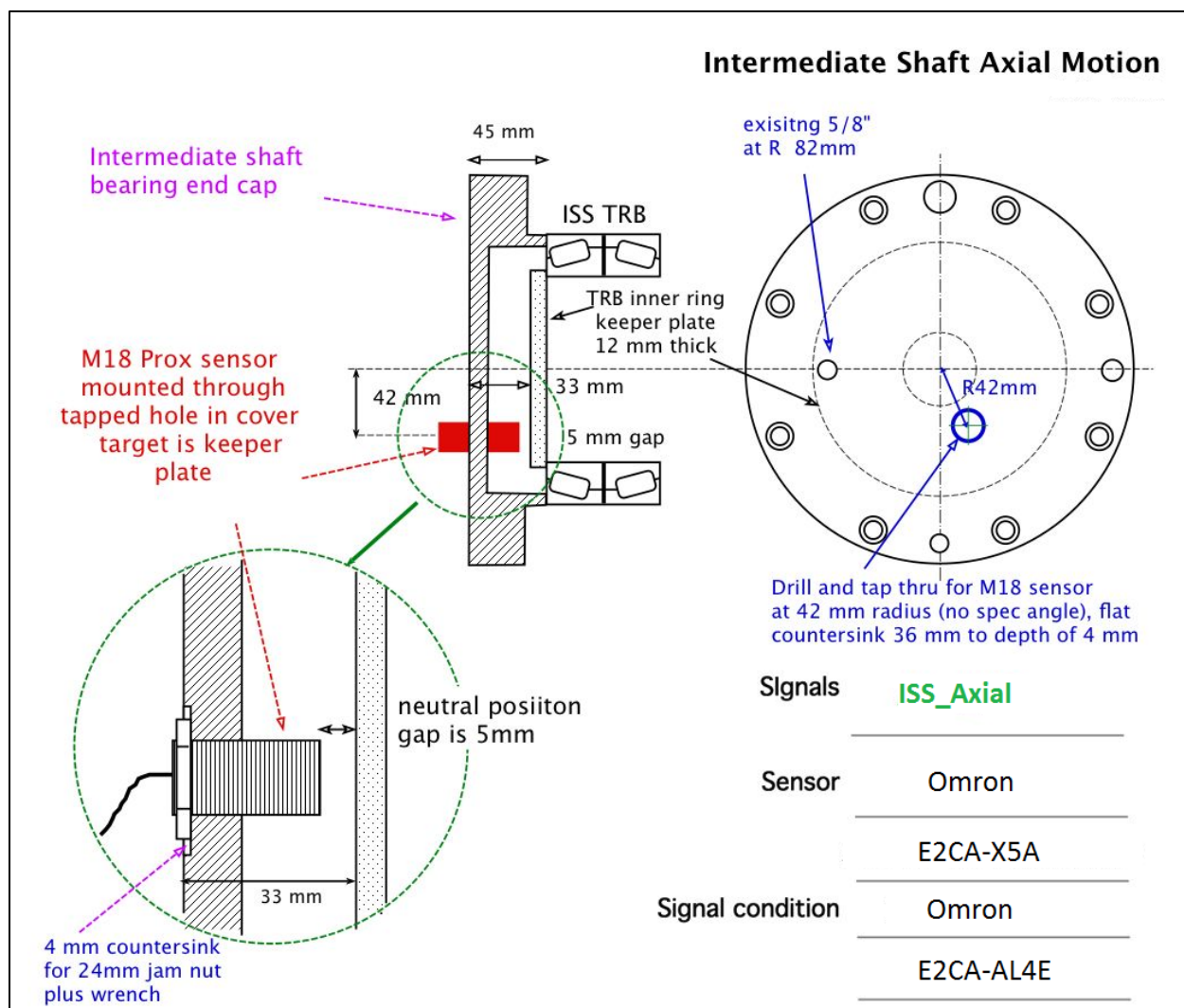**Figure 28. Ring gear external face-width load distribution**

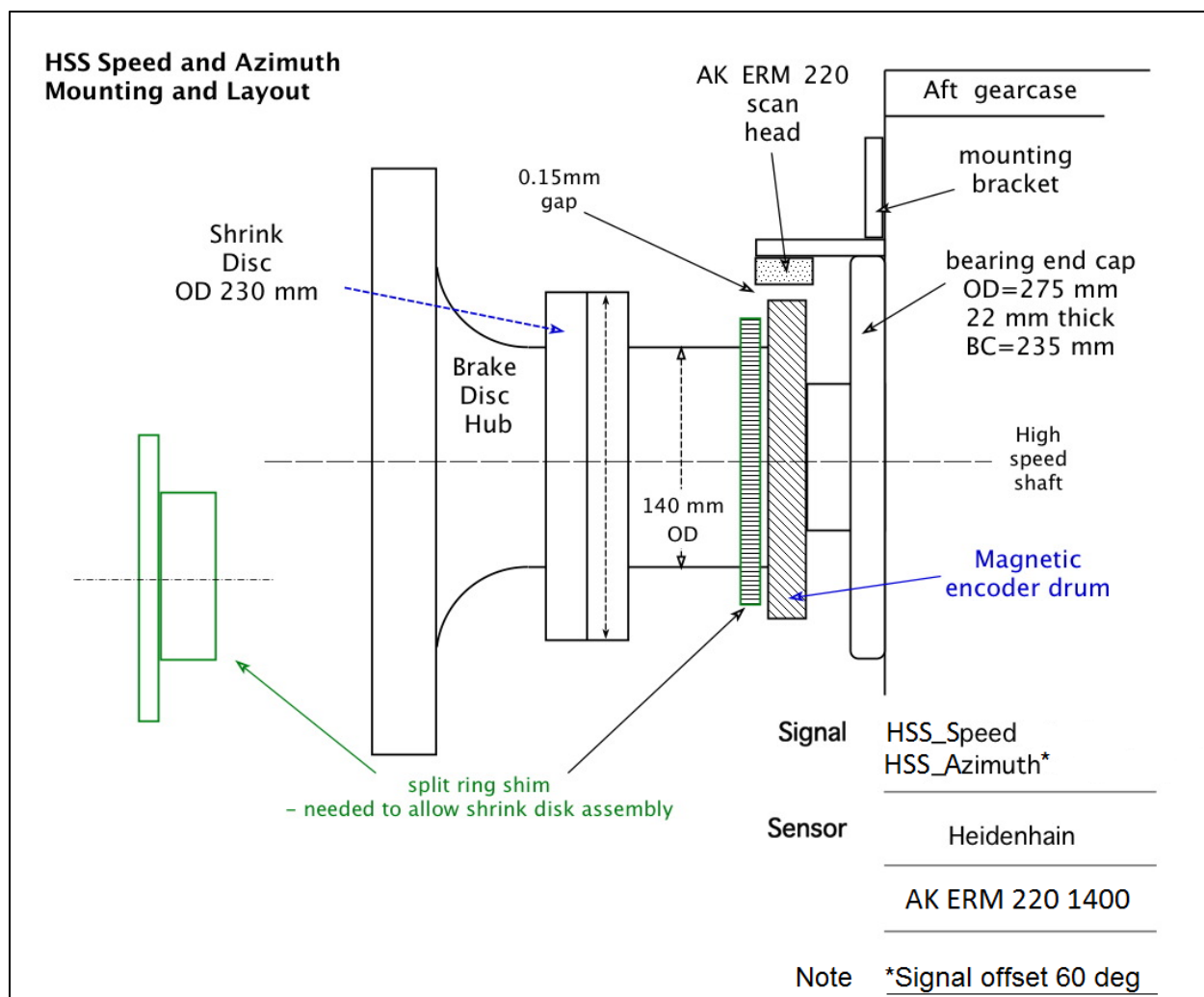**Figure 29. Intermediate-shaft axial motion**

Figure 30. HSS speed and azimuth

GEARBOX EXAMINATION #2

1 Introduction and Background

Many gearboxes in wind turbines do not achieve their expected design life [1]; they do, however, commonly meet or exceed the design criteria specified in current standards in the gear, bearing, and wind turbine industry as well as third-party certification criteria. The cost of gearbox replacements and rebuilds, as well as the downtime associated with these failures, increases the cost of wind energy. In 2007, the U.S. Department of Energy established the National Renewable Energy Laboratory (NREL) Gearbox Reliability Collaborative (GRC). Its goals are to understand the root causes of premature gearbox failures and to improve their reliability [2]. The GRC is examining a hypothesis that the gap between design-estimated and actual wind turbine gearbox reliability is caused by underestimation of loads, inaccurate design tools, the absence of critical elements in the design process, or insufficient testing.

The GRC uses a combined gearbox testing, modeling, and analysis approach. To date, it has focused on a 750-kilowatt (kW) drivetrain, including the dedicated design of a nonproprietary gearbox with cylindrical roller bearings (CRBs) in the planetary section. Two of these gearboxes, GB1 and GB2, were manufactured and tested. Phase-1 and Phase-2 testing focused on planetary section load-sharing characteristics [2]. A major finding was the detrimental effect of rotor nontorque loads (NTLs) on load sharing, predicted fatigue life in high-torque conditions, and the risk of bearing skidding in low-torque conditions [3]. The GRC has disseminated engineering drawings, gearbox models, test data, and results [4], which have facilitated improvements to gearbox design standards and associated modeling tools. More recently, additional dynamometer tests in Phase 3 were conducted [5,6] with additional instrumentation on the high-speed shaft
(HSS) and its locating tapered roller bearing (TRB) pair [7,8]. The objective of these tests was to assess HSS TRB load-sharing characteristics with a misaligned generator [9-11] and the potential for roller slipping during transient and grid loss events [12,13].

Simultaneous with the Phase-3 testing on the original GRC gearbox design, the GRC gearbox was redesigned to improve its load-sharing characteristics and predicted fatigue life. This new gearbox is referred to as GB3. The redesign was led by Romax Technology with contributions from Powertrain Engineers and The Timken Company (hereafter referred to as Timken). The most important aspect of the redesign was to replace the CRBs with preloaded TRBs in the planetary section [14-17], resulting in a projected increase of three times the planetary section fatigue life compared to the previous design [18]. Brad Foote Gearing assembled the gearbox.

This report describes the recently completed tests of GRC GB3 in the National Wind Technology Center (NWTC) dynamometer and documents any modifications to the original test plan [19]. In this manner, it serves as a guide for interpreting the publicly released data sets [20] with brief analyses to illustrate the data. The primary test objective was to measure the planetary load-sharing characteristics in the same conditions as the original GRC gearbox design. If the measured load-sharing characteristics are close to the design model, the projected improvement in planetary section fatigue life and the efficacy of preloaded TRBs in mitigating the planetary bearing fatigue failure mode will have been demonstrated. Detailed analysis of that test objective will be presented in subsequent publications.

2 Test Article

The GRC drivetrain was originally designed for a stall-controlled, three-bladed turbine with a rated power of 750 kW [2]. The drivetrain generates electricity at two main shaft speeds: 14.7 rpm and 22.1 rpm. The gearbox ratio of 81.491 converts these main shaft speeds to generator speeds of 1,200 rpm and 1,800 rpm. The drivetrain design follows a conventional configuration in which the main bearing and main shaft, gearbox, and generator are mounted to the bed plate as shown in Figure 1. The main shaft is connected to the gearbox via a shrink disk and the gearbox is connected to the generator via a flexible coupling. The gearbox is mounted with a three-point configuration in which forces are reacted mostly at the main bearing, whereas rotor moments and torque loads are transferred to the bed plate through two torque arms.
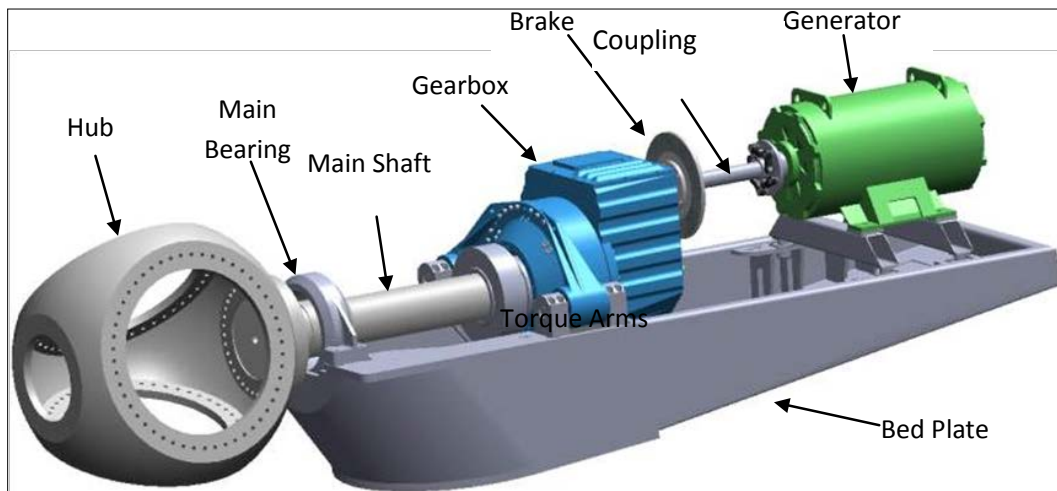
Figure 1. Drivetrain configuration

The GRC gearboxes are composed of one low-speed planetary stage with three planet gears and two parallel shaft stages as shown in Figure 2. The housing components of the original Jahnel-Kestermann PSC 1000-48/60 commercial gearboxes were retained, but the majority of the internal components were redesigned and newly manufactured for all of the GRC gearboxes.

Figure 2. Gearbox configuration. *Illustration by Powertrain Engineers Inc.*

2

A tradeoff study was completed for the GB3 design to determine what planetary system changes had the most beneficial impact on predicted fatigue life [14-17]. After a down-selection process, which considered cost and schedule impacts, the following key improvements were selected:
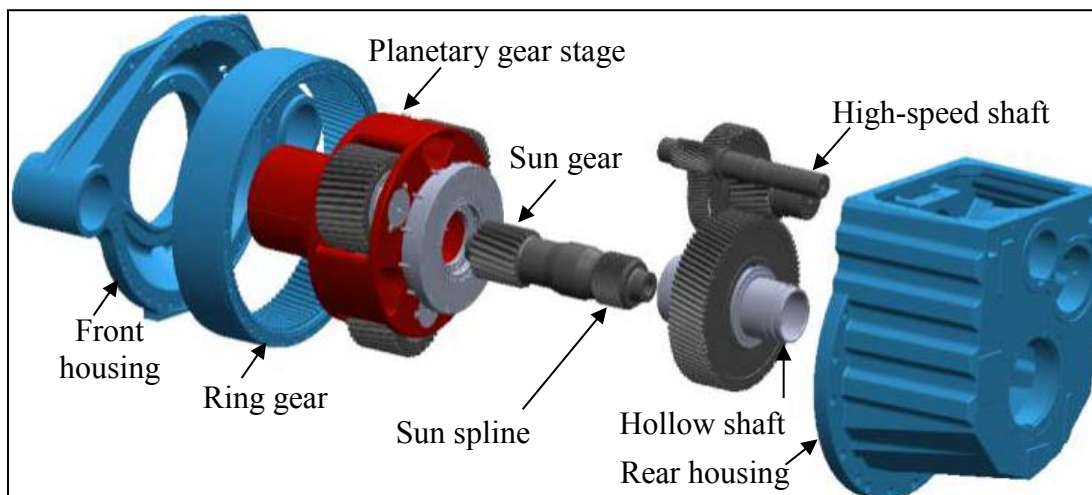
- Preloaded planet carrier and planet TRBs, and stiffer planet pins to improve alignments in the planetary system and improve the load-sharing characteristics

- Planet TRB outer races integral to the planet gears to increase capacity and eliminate outer race fretting. The planet TRBs still utilize an inner race containing instrumentation, resulting in an overall semi-integrated planet bearing design

Additional design changes were also made to facilitate the key improvements, or otherwise improve assembly or operation of the gearbox. Although valuable, the following changes were not part of the test verification process:

- A robust bolt system between the ring gear and front and rear housings to accommodate increased axial loads from the planetary system

- A ring gear nitrided to improve fatigue life. The ring gear is also 29 mm longer to improve ease of assembly of the central plate and allow more space for the TRBs and the new oil feed ring system. This change necessitated shifting the generator aft by the same amount by enlarging the mounting holes in the generator-mount cross members

- The spline coupling crowning was reduced by 50% to increase the load-carrying area of the spline without negatively affecting system life or gear alignment

- Hollow shaft bearings in an X-arrangement with tighter inner races to reduce fretting

- An improved, semidry sump lubrication system with improved delivery to the planet bearings, planet gears, and HSS TRBs.

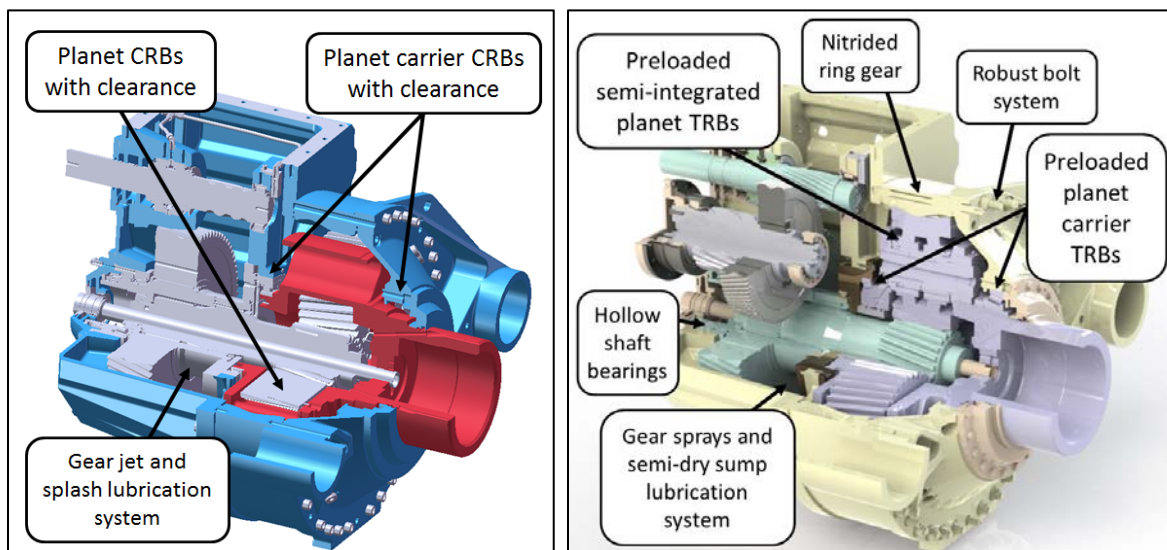A comparison of the key characteristics of both GRC gearbox designs is shown in Figure 3.

Figure 3. Comparison of GB2 (left) and GB3 (right) design characteristics. *Illustration by Romax Technology (right)*

3

3 Test Environment

The National Wind Technology Center (NWTC) 2.5-megawatt (MW) dynamometer test facility [21] was used for GB3 testing. The dynamometer variable frequency drive and NTL system enabled the reproduction of field conditions. The dynamometer variable frequency drive enables dynamic torque control up to a bandwidth of 250 hertz (Hz). The NTL system can apply thrust, vertical force, and lateral force to the adapter couplings in front of the GRC main bearing as shown in Figure 4. Given the fixed distance between the NTL application point and the GRC main bearing, the relationship between these vertical and lateral forces and the resulting pitch or yaw moments on the GRC main shaft is fixed and cannot be controlled independently. The NTL system can apply loads dynamically up to approximately 10 Hz, depending on force and hydraulic flow volume requirements. GB3 installed in the drivetrain is shown in Figure 5.

Figure 4. Drivetrain dynamometer installation. *Photo by Jonathan Keller, NREL 40428*
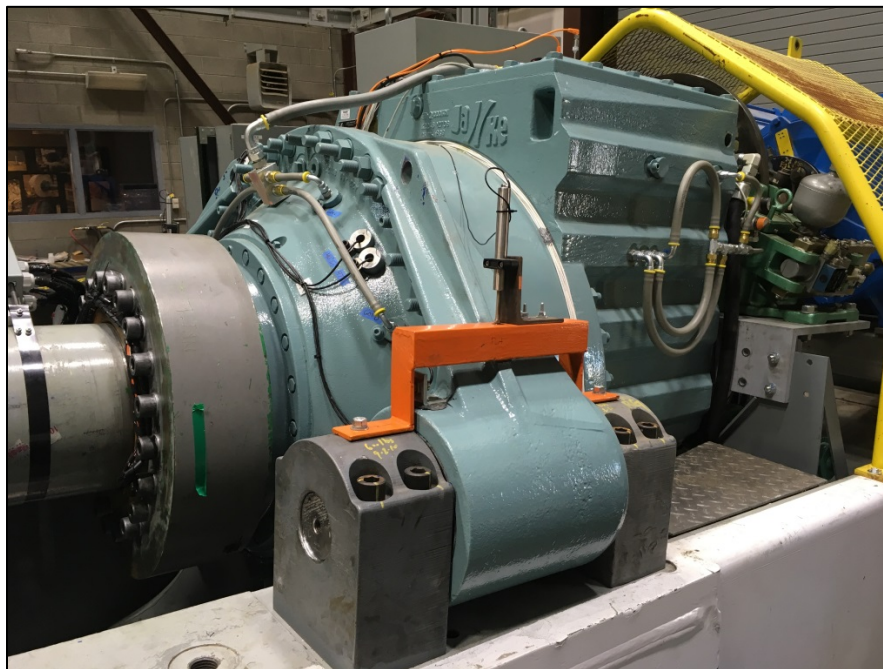
Figure 5. GB3 installation. *Photo by Jonathan Keller, NREL 40430*

4

The data acquisition system (DAS) was based on the National Instrument's deterministic Ethernet platform. One set of chassis processed rotating planetary section signals and was mounted in an enclosure on the main shaft. The output of that system was converted to fiber optic signals and sent back through the conduit tube in the center of the gearbox low-speed shaft. A fiber optic rotary joint at the rear of the gearbox then converted the signals to the nonrotating frame. A second set of chassis processed other fixed frame signals and all of the HSS signals. The DAS and chassis are shown in Figure 6.

Figure 6. Data acquisition system. *Photo by Mark McDade, NREL 40432*

5

4 Instrumentation

Detailed descriptions for all instrumentation are included in the test plan [19]. For reference, instrumentation for Phase 3 testing of GB3 is categorized by location of the sensor, as listed below.

- Dynamometer

- Nontorque loading system

- Main shaft

- Gearbox

    o Housing

    o Ring gear

    o Planet carrier

    o Planet gears

    o Planet bearings

    o Sun gear

    o Low-speed shaft (LSS) bearings

    o Intermediate-speed shaft bearings

    o High-speed shaft

    o High-speed shaft bearings

- Lubrication system

- Controller.

4.1 Instrumentation Changes and Deviations

After installation and initial commissioning, some deviations from the planned instrumentation were discovered. Those deviations are summarized here and, where necessary, described further in the following sections.

The zero-point of the main shaft azimuth measurement (signal name LSS_Azimuth) derived from an encoder installed on the fiber optic slip ring, the azimuthal location of the strain gages rotating on the main shaft (signal names MSBM_YY and MSBM_ZZ), and the azimuthal location of any planet do not coincide with each other. That is, each has an azimuthal offset that is best determined after the main shaft and encoder are installed to the gearbox. To determine these offsets, data was acquired while the gearbox was stationary and the planet and main shaft positions were examined. In this manner, the offset of the main shaft azimuth to the main shaft strain gages was determined to be $\phi_0 = 113°$. That is, the rotor bending moments in the fixed frame (signal names MSBM_y and MSBM_z) can be determined from the rotating measurements by

6

$$\text{MSBM\_y} = -\text{MSBM\_YY}\sin(\text{LSS\_Azimuth} - \phi_0) - \text{MSBM\_ZZ}\cos(\text{LSS\_Azimuth} - \phi_0)$$
$$\text{MSBM\_z} = +\text{MSBM\_YY}\cos(\text{LSS\_Azimuth} - \phi_0) - \text{MSBM\_ZZ}\sin(\text{LSS\_Azimuth} - \phi_0) \tag{1}$$

Examining the stationary data set shows a negative fixed frame pitch moment, M_y = -69 kilonewton meter (kNm) and a near zero fixed frame yaw moment, M_z =1 kNm, confirming this offset. In this position, the measured main shaft azimuth was 56.3° and planet A was close to the top of the ring gear. By examining the strain at the top of the ring gear in operation, it was determined that the actual offset of planet A from the top of the ring gear is approximately 84°. That is, when the measured main shaft azimuth is 84°, planet A is at the 0° circumferential location, planet B is at the 240° location, and planet C is at the 120° location. Similarly, the HSS azimuth measurement (signal name HSS_Azimuth) also contains an offset because of its mounting. For both GB2 and GB3, the offset is 60° [6].

More notably, one of the planet bearing strain gages (signal name PlanetB_LOAD_DW_77) was not operational. Presumably, it was damaged during either the assembly, shipping, or installation process of the gearbox. Although nonoperational, it remained a part of the data stream. For curve fitting of the bearing load zone, it can reasonably be assumed that this measurement is the same value as the measurement on the opposite side of the load zone (signal name PlanetB_LOAD_DW_323) as illustrated in the next section. Additionally, two other strain gages on the same planet (signal names PlanetB_LOAD_DW_20 and PlanetB_LOAD_DW_285) appear to have been swapped or otherwise labeled incorrectly as shown in the next section. They retain their original, expected data labels in the data stream.

Additionally, the temperature measurements on the inner rings of the HSS bearings (signal names TEMP_HSS_TRB_IR_UW and TEMP_HSS_TRB_IR_DW), which are transmitted through a slip ring on the HSS, became highly variable and provided unrealistic values in the latter portion of testing. The strain gage measurements on the HSS did not seem to be affected, however. Lastly, the indicator of the generator's electrical connection to the grid at low power (signal name Controller_g_contactor) listed in the test plan was also not operational nor was it part of the data stream.

4.2 Signal List

Data was recorded in two separate data streams. A 100-Hz rate was used to record information on the planetary and intermediate sections of the gearbox. A 2,000-Hz rate was used to record information on the high-speed section of the gearbox. Relevant signals related to the input loading conditions, lubrication, or output performance of the generator and controller were also recorded. Many signals were measured in engineering units, whereas others were recorded in units of millivolts per volt (mV/V). The signals included in each data stream are listed in Table A-1 and Table A-2 in Appendix A, for the 100-Hz and 2,000-Hz rates, respectively.

The data files were named beginning with the convention "Test Type_," derived from the name of a particular test in the test plan such as "Static_NTL." "Test Sequence_" follows Test Type and corresponds to sequences in the test plan such as "5A." Finally, the data file names were appended with "YYYY_MM_DD_HH_SS_ZZZZHz.tdms," in which YYYY, MM, DD, HH, and SS are the year, month, date, hour, and second of the data acquisition, respectively, and ZZZZ is the acquisition rate in hertz.

5 Test Sequence

Testing of GB3 in Phase 3 consisted of the following major test sequences:

- Drivetrain recommissioning
- NTL tests
- HSS radial misalignment tests
- Field-representative tests
- Variable-speed tests.

5.1 Drivetrain Commissioning

The drivetrain commissioning test sequence ensured that the dynamometer controls, drivetrain, gearbox, lubrication and cooling systems, and instrumentation were all operating normally and ready for full-load testing. Throughout the commissioning process examples of data were reviewed and the instrumentation signals were corrected as necessary. Data sets were also gathered in nonoperational (static) states to record signal offsets. The gearbox first underwent flushing, followed by a break-in sequence during which the sensors and controls were verified while gradually increasing speed, torque, and nontorque loads.

5.1.1 Gearbox Flushing

Commissioning began on Sept. 14, 2016, by flushing the gearbox to remove contaminants that might have been left over from the manufacturing and assembly process. The gearbox oil was heated to over 45°C and the lubrication system was operated to flush the oil through the gearbox, small particle filter, and oil particle counter until it reached a cleanliness of -/14/11. The dynamometer was then engaged and the gearbox was spun at low speed (5% to 10% rated speed or 1 to 2 rpm) while continuing to flush the oil.

5.1.2 Gearbox Run-In

The objective of "running-in" the gearbox, listed in Table 1, was to reduce the roughness of mating surfaces created by the manufacturing process. The run-in procedure was completed between Sept. 14 and 19, 2016. During the process, inconsistencies in the torque and power signals were noted and corrected, requiring two separate runs in some cases.

Table 1. Gearbox Run-In Procedure

Date	Load Step	Drivetrain Speed (%)	Torque (%/kNm)	Duration (hr)	Oil Sump Temp (°C)	Oil Cleanliness
Sept. 14	1	30	5/18	1.0	43	-/14/10
Sept. 14-15	3	100	5/18	2.5	55	-/15/11
Sept. 16	4a	100	20/72	1.5	52	-/15/10
Sept. 16	5a	100	40/144	2.0	54	-/14/9
Sept. 16	6a	100	60/216	0.5	65	-/15/11
Sept. 16	7a	100	80/288	0.5	64	-/15/11
Sept. 16-19	8a-b	100	100/360	4.5	66	-/15/10

8

At each load step, the oil sump and bearing temperatures were stabilized and the oil cleanliness level were better than -/15/12. After the last load step, all oil filters were replaced.

5.1.3 High-Speed Shaft Torque Investigation

In previous testing of GB2, a periodic ±10% variation in the HSS torque was measured—even in offline conditions [6-7,10]. A possible source for this variation has been hypothesized as tooth spacing errors on the high-speed pinion [22]. Because the high-speed pinion was newly manufactured for GB3, there was an opportunity to examine this hypothesis by repeating previous GB2 testing. The test sequence listed in Table 2 was completed on Oct. 4, 2016.

Table 2. HSS Torque Investigation Tests

Date	Power (%/kW)	Drivetrain Speed (%)	HSS Speed (rpm)
Oct. 4	Offline	16.7	300
Oct. 4	Offline	33.3	600
Oct. 4	Offline	50	900
Oct. 4	Offline	66.7	1,200
Oct. 4	12%/90	66.7	1,200
Oct. 4	25%/188	66.7	1,200
Oct. 4	Offline	83.3	1,500
Oct. 4	Offline	100	1,800
Oct. 4	25%/188	100	1,800
Oct. 4	50%/375	100	1,800
Oct. 4	75%/563	100	1,800
Oct. 4	100%/750	100	1,800

HSS bending moments and torque can be calculated in an identical manner as GB2 testing [7], updated to reflect the gage factors and offsets in the data that are specific to GB3 [23].

$$M = \frac{\pi \left(D^4 - d^4 \right) E}{32 D G_M} \frac{dV}{V} = K_M \frac{dV}{V} + b_m \tag{2}$$

$$T = \frac{\pi \left(D^4 - d^4 \right) E}{16 D G_T \left(1 + \upsilon \right)} \frac{dV}{V} = K_T \frac{dV}{V} + b_T \tag{3}$$

Updated dimensional and material characteristics of the HSS and instrumentation are listed in Table 3 and the resulting calibration coefficients and data offsets are listed in Table 4. Negative scale factors relate to particular wiring of the strain gage bridges. Bending moment offsets were determined by eliminating the average bending moment for the full power case, whereas the torque offset was determined from the static, nonoperational test data. The net torque calculated with this process is positive and is in terms of the torque that the HSS applies to the generator.

9

Table 3. HSS and Instrumentation Properties

Inner Diameter	Outer Diameter	Modulus of Elasticity	Poisson's Ratio	Bending Gage Factor	Torque Gage Factor
d	D	E	υ	G_M	G_T
(m)	(m)	(GPa)			
0.025	0.1	207	0.3	2.155	2.135

Table 4. HSS Bending and Torque Coefficients and Offsets

Signal	Scale Factor (kNm/mV/V)	Offset (kNm)
HSS_UY_BM	-9.399	-0.139
HSS_UZ_BM	9.399	0.079
HSS_DY_BM	-9.399	0.206
HSS_DZ_BM	9.399	0.004
HSS_exY_BM	-9.399	-0.327
HSS_exZ_BM	9.399	-0.383
HSS_TQ	-14.596	0.072

The measured torque data at rated speed for each gearbox is shown in Figure 7. In each condition, data was acquired over 30 shaft revolutions. Although the absolute torque levels for the gearboxes differ slightly, the overall pattern is clear. The HSS torque variation evident in GB2 has largely been eliminated in GB3.
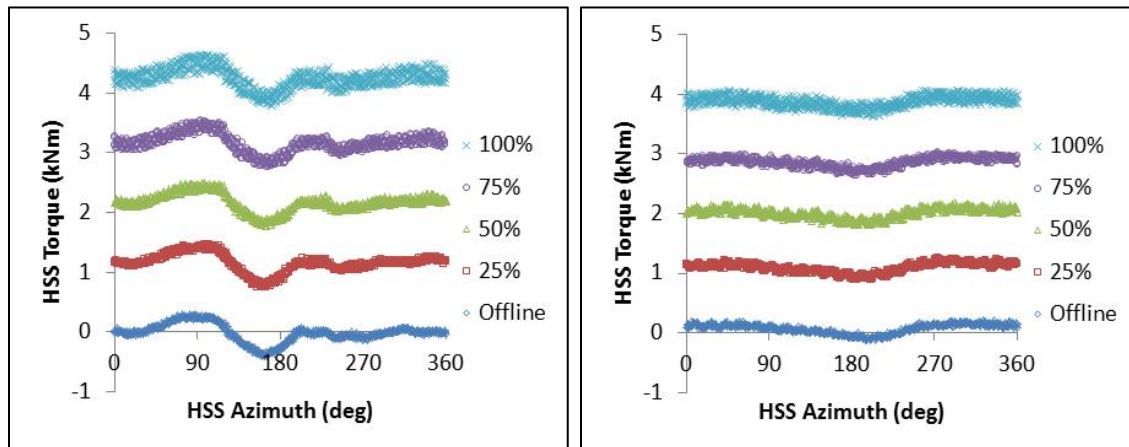
Figure 7. HSS torque at 1,800 rpm for GB2 (left) and GB3 (right)

5.2 Nontorque Load Tests

Phase 3 testing of GB3 repeated the sequence of NTL tests for direct comparison to GB2, with additional data acquisitions at high NTL levels to assess data repeatability. The NTL tests proceeded from simple static bending moments, through simple dynamic bending moments, to static thrust load testing. The following sections describe each test series.

10

5.2.1 Static Bending Moment

Static bending moment tests for GB3 were conducted in offline conditions (sequences 1–3), and at 25% power (sequence 4), 50% power (sequence 5), 75% power (sequence 6), and 100% power (sequence 7) conditions. Similar to testing on GB2, additional test data were acquired at 10% power in a final sequence (sequence 8). The operating conditions for these sequences are summarized in Table 5, which also references specific bending moment conditions provided in Table 6. The static bending tests were performed from Sept. 21 to Sept. 29, 2016.

Table 5. Static NTL Tests

Date	Test Number	Power (%)	Speed (%)	Rotation Direction	NTL Sequences
Sept. 21	1	Offline	5.5	Normal	A1,H1
Sept. 28	2	Offline	5.5	Reverse	A1,H1
Sept. 23	3	Offline	100	Normal	All
Sept. 26	4	25	100	Normal	All
Sept. 22	5	50	100	Normal	All
Sept. 28-29	6	75	100	Normal	All
Sept. 21	7	100	100	Normal	All
Sept. 22	8	10	100	Normal	A1,H1

Table 6. Static NTL Sequences

NTL Sequence	Myy (kNm)	Mzz (kNm)	Increment (kNm)
A1	-300 to 300	0	100
B	-300 to 300	-100	100
C	-300 to 300	-200	100
D	-300 to 300	-300	100
A2	-300 to 300	0	100
E	-300 to 300	100	100
F	-300 to 300	200	100
G	-300 to 300	300	100
A3	-300 to 300	0	100
H1	0	-300 to 300	100
H2	0	300 to -300	100

All cases were performed with respect to the tared (i.e., zero-bending-moment) condition, which changes slightly with drivetrain power. When tared, the pitch moment caused by the weight of the dynamometer couplings and shafting has been removed from the drivetrain. That is, tests with zero bending moment are in a pure-torque condition. Figure 8 shows an example of the test conditions that were achieved at rated power. Some of the most severe, combined pitch and yaw moment cases were not achieved because of overall limits of the actuator forces. These cases correspond to when the actuators must provide the vertical force required to first tare the drivetrain plus additional vertical or lateral forces required to achieve a large moment.
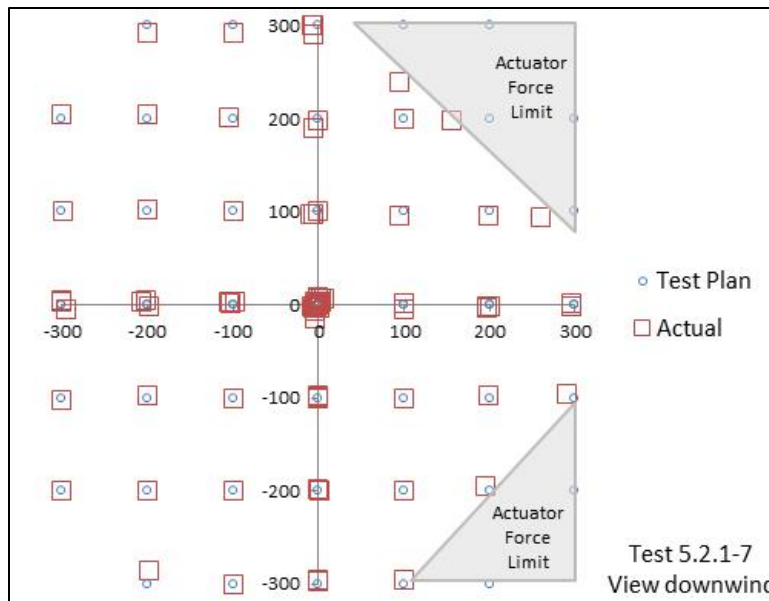
11

Figure 8. Static bending moments at 100% power

Three cycles of roller passages over several example planet B bearing strain gage measurements for the full-power, pure-torque case are shown in Figure 9 and Figure 10. Measured planet bearing strains can be converted to bearing load in kilonewton (kN) by examining the strain range along with the calibration factors that were measured in a special test rig [24]. The larger the strain range, the larger the bearing load at that measurement location. Offsets of each signal have been adjusted to make the strain range clearer.
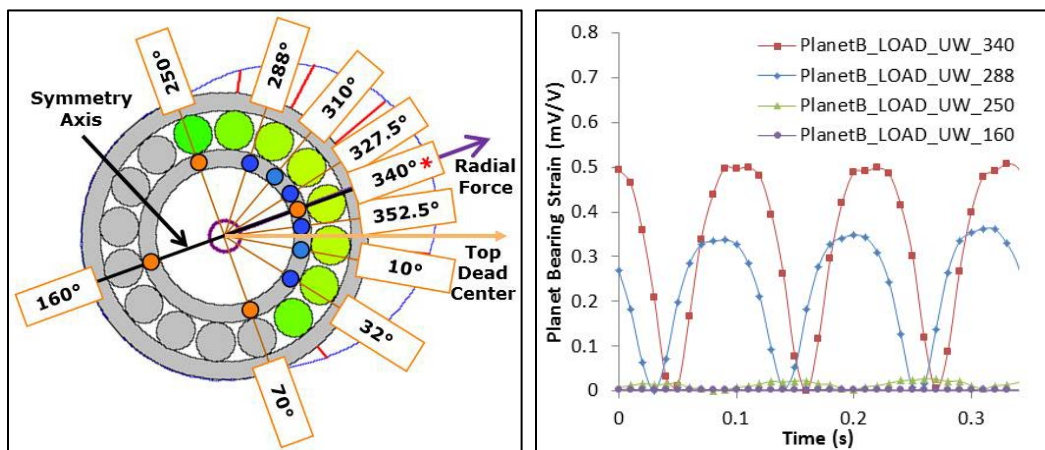

Figure 9. Planet B upwind bearing load zone (left) and measurements (right) at 100% power
Illustration by Timken (left)

For the upwind (UW) bearing, Figure 9 shows the highest loaded location at the expected center of the load zone (PlanetB_LOAD_UW_340) aligned with the radial force direction, a less loaded location in the outer half of the load zone (PlanetB_LOAD_UW_288), a very lightly loaded location at one of the edges of the expected load zone (PlanetB_LOAD_UW_250), and the unloaded location opposite the expected center of the load zone (PlanetB_LOAD_UW_160). The magnitudes of the resulting measurements are as expected; highest in the center of the load zone, much lower at the edges, and essentially zero opposite the load zone.

12

A similar example of the planet B downwind (DW) bearing strain gage measurements are also shown in Figure 10. Here, however, the measurement location at the expected center of the load zone (PlanetB_LOAD_DW_20) has a smaller magnitude than the other measurements in the load zone and the measurement location at the expected edge of the load zone (PlanetB_LOAD_DW_285) has the largest magnitude. By examining all the measurements for the planet B downwind bearing, the only reasonable explanation is that these two measurements were swapped. The unloaded location opposite the expected center of the load zone (PlanetB_LOAD_DW_200) has very little measured strain, as expected. Lastly, the two locations in the outer half of the load zone (PlanetB_LOAD_DW_323 and PlanetB_LOAD_DW_77) are also compared. These two measurements should be very similar in magnitude. However, upon further examination, one of them (PlanetB_LOAD_DW_77) has a value of exactly zero at all times in all acquisitions. Thus, for analysis purposes and curve fitting of the load zone this signal can be reasonably assumed to be equal to its counterpart (PlanetB_LOAD_DW_323). All analyses conducted hereafter assume this configuration as mentioned previously in Section 4.1.
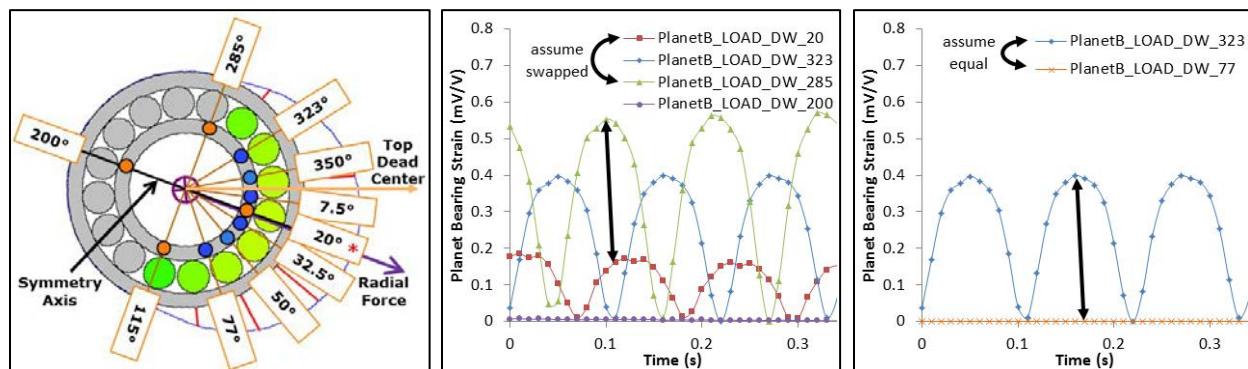
Figure 10. Planet B downwind bearing load zone (left) and measurements (center and right) at 100% power. *Illustration by Timken (left)*

5.2.2 Dynamic Bending Moment

Dynamic bending moment tests were completed in offline (sequence 1), 25%-power (sequence 2), and 100%-power (sequence 3) conditions on Oct. 21, 2016. The operating conditions for these sequences are summarized in Table 7, which also references specific NTL loading conditions provided in Table 8.

Table 7. Dynamic NTL Tests

Date	Test Number	Power (%)	Speed (%)	NTL Sequences
Oct. 21	1	Offline	100	All
Oct. 21	2	25	100	All
Oct. 21	3	100	100	All

13

Table 8. Dynamic NTL Sequences

NTL Sequence	Myy (kNm)	Mzz (kNm)	Frequency (Hz)
A	0 to -50	0	2
D	0 to -200	0	2
G	0	0 to 50	2
R	0	-100 to 100	2

5.2.3 Static Thrust

Static thrust test sequences were completed on Oct. 21, 2016, in offline mode (sequence 2), at 25%-power (sequence 3), 50%-power (sequence 4), 75%-power (sequence 5), and 100%-power (sequence 6) conditions as listed in Table 9.

Table 9. Static Thrust Tests

Date	Test Number	Power (%)	Speed (%)	Thrust (kN)	Increment (kN)
Oct. 21	2	Offline	100	0 to -100 to 100 to 0	50
Oct. 21	3	25	100	0 to -100 to 100 to 0	50
Oct. 21	4	50	100	0 to -100 to 100 to 0	50
Oct. 21	5	75	100	0 to -100 to 100 to 0	50
Oct. 21	6	100	100	0 to -100 to 100 to 0	50

5.3 Generator Misalignment Tests

New instrumentation on the GB3 HSS measures bearing temperature on the inner and outer rings of the TRB pair. The aligned and maximum misalignment (3º) conditions of the coupling shaft to the generator were tested in the offline mode (sequence 1 and 2), at 25%-power (sequence 3), 50%-power (sequence 4), 75%-power (sequence 5), and 100%-power (sequence 6) conditions listed in Table 10. Aligned tests were completed on Oct. 21, 2016, whereas misaligned tests were completed on Nov. 22, 2016.

Table 10. Generator Misalignment Tests

Test Number	Power (%)	Speed (%)	Misalignment (°/mm)
0	Offline	0	0/0 and 3°/32.06
1	Offline	5.5	0/0 and 3°/32.06
2	Offline	100	0/0 and 3°/32.06
3	25	100	0/0 and 3°/32.06
4	50	100	0/0 and 3°/32.06
5	75	100	0/0 and 3°/32.06
6	100	100	0/0 and 3°/32.06

14

Figure 11 shows the measured temperature differentials between the inner and outer rings for the HSS bearings over a range of drivetrain power settings. Because the downwind bearing carries both axial and radial load its temperature difference ranges between 20 and 27°C, higher than the 8–10°C temperature difference for the more lightly loaded upwind bearing. Bearing temperatures increase slightly with drivetrain power. The temperature of the oil at the bearing manifold was held nearly constant between 48.5 and 50°C by the oil cooling system. These measured temperature differentials are within the typical range given in the International Electrotechnical Commission's 61400-4 gearbox design standard. The results shown in Figure 11 were collected during the aligned tests on Oct. 21, 2016, whereas the inner ring measurements were consistent. Testing results after Oct. 21, 2016, display high variability and unrealistic values for the inner ring temperatures.
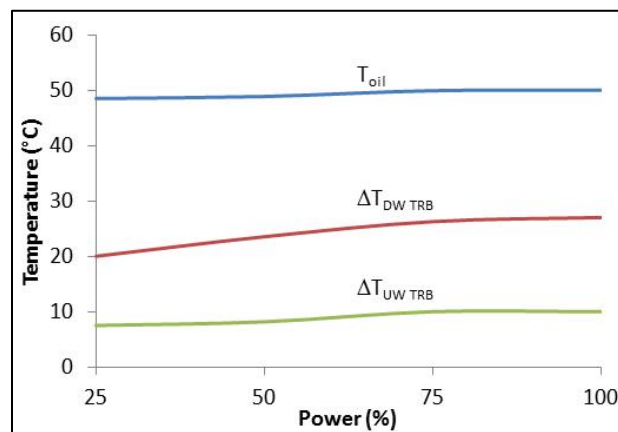

Figure 11. HSS bearing ring temperature differentials

5.4 Field-Representative Tests

Examples of field-representative testing completed in Phase 3 are discussed in the following sections. These examples correspond to normal power production and shutdown cases, respectively. Normal power production cases utilized the dynamometer variable-frequency drive and the dynamic capability of the NTL system, whereas the shutdown cases utilized the GRC drivetrain mechanical braking system.

5.4.1 Normal Power Production

Normal power production cases representing 5-meters per second (m/s), 15-m/s, and 25-m/s wind speed cases were tested. In each case, a system identification test was performed in which the desired dynamic torque is commanded and the actual torque is measured. This measured response is then used to tailor the commanded dynamic torque to result in a main shaft torque close to the values measured in the field. The NTLs were operated in force-feedback mode. The test for each wind speed case lasted 11 minutes, including a 30-second (s) ramp-up period to full load at the beginning of the test and a 30-s ramp-down period at the end of the test.

The normal power production cases were completed on Dec. 6, 2016. The tests proceeded in a graduated fashion, beginning with the low torque and NTLs for the 5-m/s wind speed case, then increasing them for the 15-m/s case, and increasing them again to near rated values for the 25-m/s case. A 10-s snapshot of the results for the 25-m/s wind speed case is shown in Figure 12.

15

The measured torque and bending moments in the dynamometer show good correlation with those measured in the field.
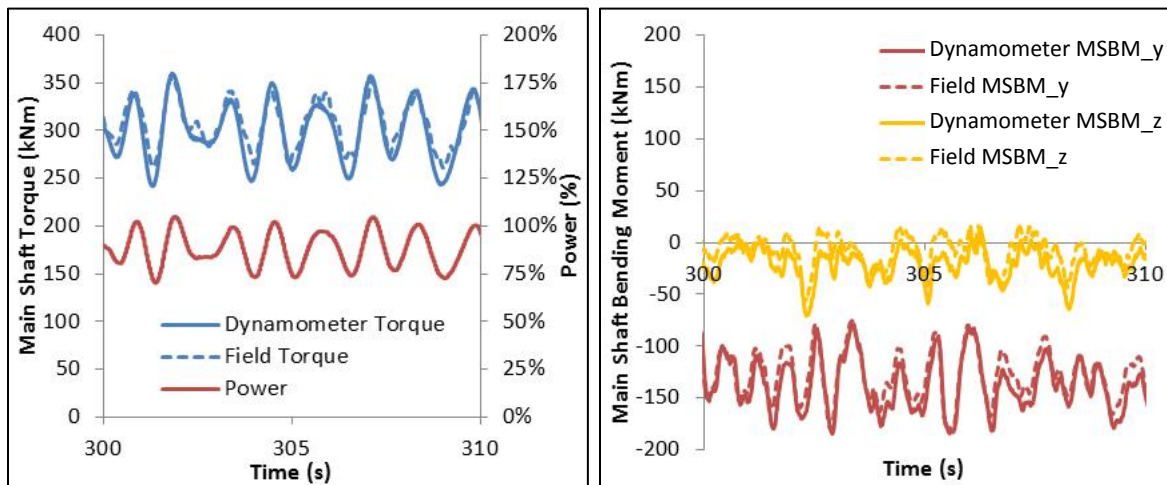

Figure 12. Main shaft torque (left) and bending moments (right) for the 25-m/s wind speed case

5.4.2 Shutdown

The GRC drivetrain uses a SIME-Stromag 3TWa37-TE2L single-caliper disk brake system. The brake disk is mounted with an interference fit to the end of the HSS. For the shutdown case, of primary interest are the loads reached immediately after engaging the disk brake.

Shutdown testing was completed on Nov. 3, 2016. The operation of the braking system hardware and software controls was verified in a graduated fashion. Each test was completed by operating the drivetrain at full speed with the generator offline, so that the initial torque was essentially zero. The power to the dynamometer was then cut off, and the system then began to slowly decelerate at a natural rate. The brake control system was programmed to actuate the brake calipers when the system crossed below a configurable speed, beginning with 1 rpm, and the resulting maximum torque value was measured. The brake application speed was then slowly increased over successive runs until the field speed of 11 rpm was reached, ensuring that the maximum torque did not exceed 200%. The final brake test in the dynamometer, where the torque reached 156% of rated, is compared in the right portion of Figure 13 to the field braking event, where the torque reached 160% of rated.
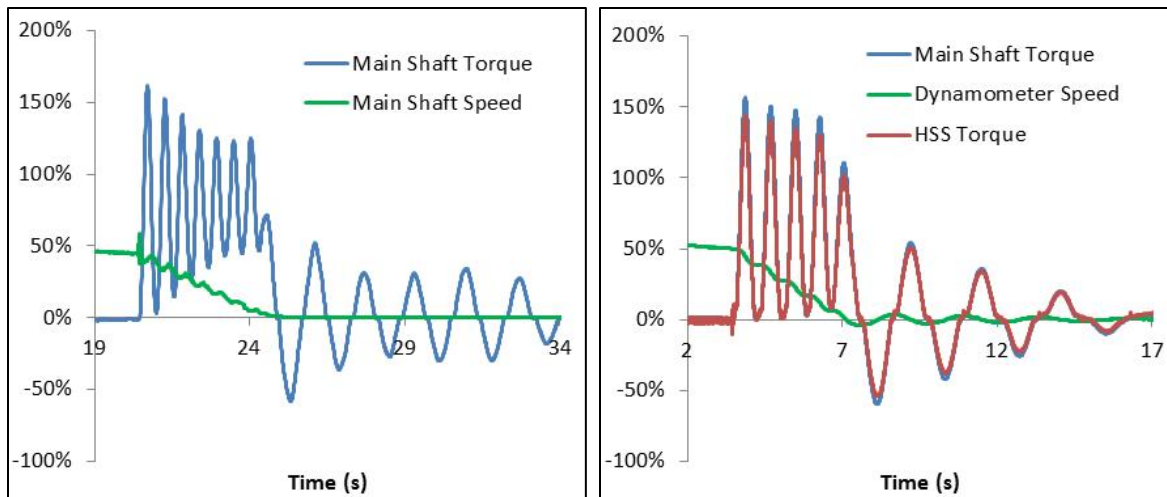
16

Figure 13. Shutdown event in the field (left) and dynamometer (right)

5.5 Grid Disconnect Tests

Controlled shutdown tests were also completed on Nov. 3, 2016. While operating at a steady-state power level, the dynamometer was intentionally shut down in a controlled fashion. The GRC generator immediately disconnects and the dynamometer ramps down at a controlled speed, taking about 3 minutes to come to a complete stop. Shutdowns were performed at 25% power, 50% power, 75% power, and 100% power levels. It should be noted that the behavior wherein the GRC controller immediately disconnects the generator from the grid is the same behavior the controller would exhibit in response to a grid event.

Example results for the shutdown from 100% power are shown in Figure 14 for 10 s of the event. At approximately 8 s, the shutdown began. The generator almost immediately disconnected, dropping to no power, and the dynamometer began a slow deceleration from full speed to approximately 85% speed at 16 s. The most interesting behavior was that of the torque data for both the main shaft and the HSS. When the generator was operating at rated power, the HSS was carrying the expected full torque. When the generator was disconnected, the torque quickly dropped and *reversed* to greater than 60% of rated and oscillated for multiple cycles, finally decaying to near zero torque at 16 s.
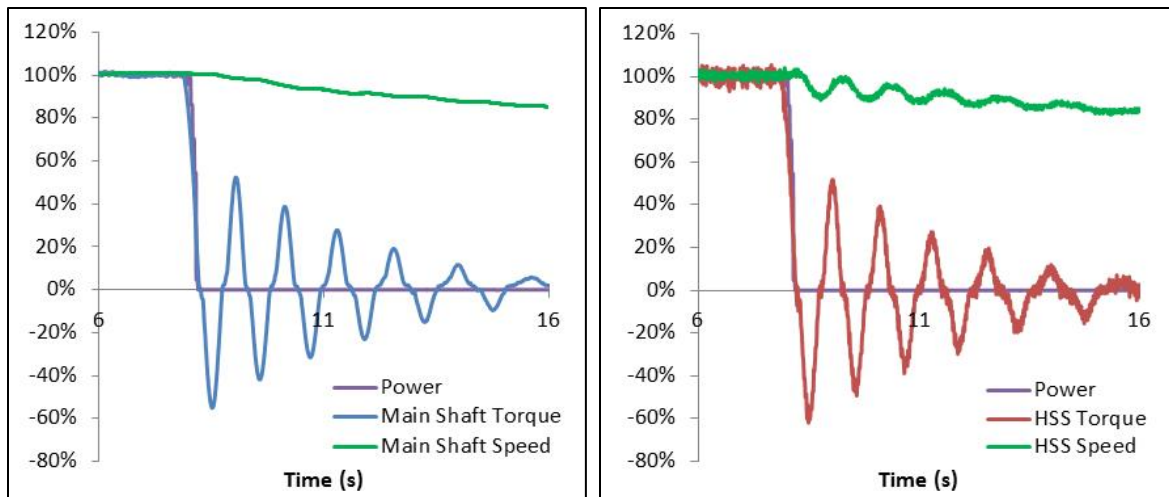
17

Figure 14. Main shaft (left) and HSS (right) response during controlled dynamometer shutdown

18

6 Summary

The GRC uses a combined testing, modeling, and analysis approach to investigate gearbox responses to specified loading conditions. Knowledge gained by comparing publicly available engineering models to measured data is disseminated to the industry, which facilitates gearbox reliability improvements. Ideally, the knowledge gained from the GRC will result in improvements to gearbox design standards and associated modeling tools.

This report describes the recent tests of the GRC GB3 in the NWTC's 2.5-MW dynamometer conducted during a few periods from September to December 2016. The primary test objective was to measure the planetary load-sharing characteristics in the same conditions as the original GRC gearbox design. If the measured load-sharing characteristics are close to the design model, the projected improvement in planetary section fatigue life and the efficacy of preloaded TRBs in mitigating the planetary bearing fatigue failure mode will have been demonstrated. The report serves as a guide for interpreting the publicly available data sets [20] with brief analyses to illustrate the tests and measured data. Detailed analysis of planetary load sharing characteristics will be presented in subsequent publications.

This report is available at no cost from the National Renewable Energy Laboratory at www.nrel.gov/publications.

ENGINEERING-PDH.COM
| MEC-151 |

References

1. Sheng, S. 2013. *Report on Wind Turbine Subsystem Reliability—A Survey of Various Databases*. NREL/PR-5000-59111. National Renewable Energy Laboratory (NREL), Golden, CO (US). http://www.nrel.gov/docs/fy13osti/59111.pdf.

2. Link, H., W. LaCava, J. van Dam, B. McNiff, S. Sheng, R. Wallen, M. McDade, S. Lambert, S. Butterfield and F. Oyague. 2011. *Gearbox Reliability Collaborative Project Report: Findings from Phase 1 and Phase 2 Testing* (Technical Report). NREL/TP-5000-51885. National Renewable Energy Laboratory (NREL), Golden, CO (US). http://www.nrel.gov/docs/fy11osti/51885.pdf.

3. Guo, Y., J. Keller and W. LaCava. 2014. *Planetary gear load sharing of wind turbine drivetrains subjected to non-torque loads*. Wind Energy, 18 (4): 757–68. doi: 10.1002/we.1731.

4. Keller, J. and R. Wallen. 2015. *Gearbox Reliability Collaborative Phase 3 Gearbox 2 Test*. NREL/TP-5000-63693. National Renewable Energy Laboratory (NREL), Golden, CO (US). doi: 10.7799/1254154. https://doi.org/10.7799/1254154.

5. Link, H., J. Keller, Y. Guo and B. McNiff. 2013. *Gearbox Reliability Collaborative Phase 3 Gearbox 2 Test Plan*. (Technical Report). NREL/TP-5000-58190. National Renewable Energy Laboratory (NREL), Golden, CO (US). http://www.nrel.gov/docs/fy13osti/58190.pdf.

6. Keller, J. and R. Wallen. 2015. *Gearbox Reliability Collaborative Phase 3 Gearbox 2 Test Report* (Technical Report). NREL/TP-5000-63693. National Renewable Energy Laboratory (NREL), Golden, CO (US). http://www.nrel.gov/docs/fy15osti/63693.pdf.

7. Keller, J. and B. McNiff. 2014. *Gearbox Reliability Collaborative High-Speed Shaft Calibration* (Technical Report). NREL/TP-5000-62373. National Renewable Energy Laboratory (NREL), Golden, CO (US). http://www.nrel.gov/docs/fy14osti/62373.pdf.

8. Keller, J., Y. Guo and B. McNiff. 2013. *Gearbox Reliability Collaborative High Speed Shaft Tapered Roller Bearing Calibration* (Technical Report). NREL/TP-5000-60319. National Renewable Energy Laboratory (NREL), Golden, CO (US). http://www.nrel.gov/docs/fy14osti/60319.pdf

9. McNiff, B., Y. Guo, J. Keller and L. Sethuraman. 2014. *High-Speed Shaft Bearing Loads Testing and Modeling in the NREL Gearbox Reliability Collaborative: Preprint.* NREL/CP-5000-63277. National Renewable Energy Laboratory (NREL), Golden, CO (US). http://www.nrel.gov/docs/fy15osti/63277.pdf.

10. Keller, J., Y. Guo and L. Sethuraman. 2016. *Gearbox Reliability Collaborative Investigation of Gearbox Motion and High-Speed-Shaft Loads*. (Technical Report). NREL/TP-5000-65321. National Renewable Energy Laboratory (NREL), Golden, CO (US). http://www.nrel.gov/docs/fy16osti/65321.pdf.

ENGINEERING-PDH.COM
| MEC-151 |

11. Keller, J. and Y. Guo. 2016. *Gearbox Reliability Collaborative Investigation of High Speed Shaft Bearing Loads*. (Technical Report). NREL/TP-5000-66175. National Renewable Energy Laboratory (NREL), Golden, CO (US). http://www.nrel.gov/docs/fy16osti/66175.pdf.

12. Helsen, J., W. Weijtjens, Y. Guo, J. Keller, B. McNiff, C. Devriendt and P. Guillaume. 2015. *Experimental Characterization of a Grid-Loss Event on a 2.5-MW Dynamometer Using Advanced Operational Modal Analysis: Preprint.* (Technical Report). NREL/TP-5000-63501. National Renewable Energy Laboratory (NREL), Golden, CO (US). http://www.nrel.gov/docs/fy15osti/63501.pdf.

13. Helsen, J., Y. Guo, J. Keller and P. Guillaume. 2016. *Experimental Investigation of Bearing Slip in a Wind Turbine Gearbox during a Transient Grid Loss Event*. Wind Energy. doi: 10.1002/we.1979.

14. Keller, J., M. McDade, W. LaCava, Y. Guo and S. Sheng. 2012. *Gearbox Reliability Collaborative Update*. NREL/PR-5000-54558. National Renewable Energy Laboratory (NREL), Golden, CO (US). http://www.nrel.gov/docs/fy12osti/54558.pdf.

15. Sheng, S., J. Keller and C. Glinksy. 2013. *Gearbox Reliability Collaborative Update*. NREL/PR-5000-60141. National Renewable Energy Laboratory (NREL), Golden, CO (US). http://www.nrel.gov/docs/fy14osti/60141.pdf.

16. Keller, J. 2014. *Wind Turbine Drivetrain Testing and Research at the National Renewable Energy Laboratory*. NREL/PR-5000-62887. National Renewable Energy Laboratory (NREL), Golden, CO (US). http://www.nrel.gov/docs/fy15osti/62887.pdf.

17. Keller, J. 2015. *Gearbox Reliability Collaborative: Gearbox 3 Manufacturing Status*. NREL/PR-5000-63869. National Renewable Energy Laboratory (NREL), Golden, CO (US). http://www.nrel.gov/docs/fy15osti/63869.pdf.

18. National Renewable Energy Laboratory. 2013. *NREL Collaborative Improves the Reliability of Wind Turbine Gearboxes*. NREL/FS-6A42-59017. National Renewable Energy Laboratory (NREL), Golden, CO (US). http://www.nrel.gov/docs/fy13osti/59017.pdf.

19. Keller, J. and R. Wallen. 2017. Gearbox Reliability Collaborative Phase 3 Gearbox 3 Test Plan (Technical Report). NREL/TP-5000-66594. National Renewable Energy Laboratory (NREL), Golden, CO (US). http://www.nrel.gov/docs/fy17osti/66594.pdf.

20. Keller, J. and R. Wallen. 2017. *Gearbox Reliability Collaborative Phase 3 Gearbox 3 Test*. National Renewable Energy Laboratory (NREL), Golden, CO (US). doi: 10.7799/1337868. https://doi.org/10.7799/1337868.

21. National Renewable Energy Laboratory. 2010. *Dynamometer Testing*. NREL/FS-5000-45649. National Renewable Energy Laboratory (NREL), Golden, CO (US). http://www.nrel.gov/docs/fy11osti/45649.pdf.

22. Houser, D. R. "Causes of GRC High Speed Shaft Dynamic Torque Variations." Presented at the NREL GRC meeting, Golden, CO, February 17–18, 2015.

23. Graeter, J. 2016. Verification Report: Installed Instrumentation Equipment at NREL NWTC. Romax Technology Report 1551-DC-004-A.

24. Keller, J. and D. Lucas. 2017. Gearbox Reliability Collaborative Gearbox 3 Planet Bearing Calibration (Technical Report). NREL/TP-5000-67370. National Renewable Energy Laboratory (NREL), Golden, CO (US). http://www.nrel.gov/docs/fy17osti/67370.pdf.

ENGINEERING-PDH.COM
| MEC-151 |

Appendix A. Data Elements

Table A-1. Elements of 100-Hz Sample Rate Data

Location	Nomenclature	Expanded Nomenclature	Units	Sensor(s)
DAS	MS Excel Timestamp	Time, MS Excel format, from Jan 1, 1900	days	DAS
DAS	LabVIEW Timestamp	Time, Labview format, from Jan 1, 1904	s	DAS
Dyno Motor	Dyno_Speed	Speed, dynamometer gearbox output converted from dynamometer motor	rpm	Calculated
Dyno GB	Dyno_Torque	Torque, dynamometer gearbox output torque spool	kNm	Strain gage
NTL	NTL_Port_Disp	Displacement, NTL port cylinder	mm	Proximity
NTL	NTL_Port_Force	Force, NTL port cylinder	kN	Load cell
NTL	NTL_Star_Disp	Displacement, NTL starboard cylinder	mm	Proximity
NTL	NTL_Star_Force	Force, NTL starboard cylinder	kN	Load cell
NTL	NTL_Thrust_Disp	Displacement, NTL thrust cylinder	mm	Proximity
NTL	NTL_Thrust_Force	Force, NTL thrust cylinder	kN	Load cell
Main shaft	LSS_TQ	Torque	kNm	Strain gage
Main shaft	MSBM_YY	Bending moment, rotating, y-axis	kNm	Strain gage
Main shaft	MSBM_ZZ	Bending moment, rotating, z-axis	kNm	Strain gage
Main shaft	MSBM	Bending moment, total	kNm	Calculated
Main shaft	MSBM_y	Bending moment, fixed, y-axis	kNm	Calculated
Main shaft	MSBM_z	Bending moment, fixed, z-axis	kNm	Calculated
Main shaft	LSS_Azimuth	Azimuth angle	degrees	Encoder
Main shaft	LSS_Speed	Shaft speed	rpm	Calculated
Housing	Trunion_Z_stbd	Displacement, gearbox Z starboard	mm	Proximity
Housing	Trunion_Z_port	Displacement, gearbox Z port	mm	Proximity
Housing	Trunion_My_bottom	Displacement, gearbox X bottom	mm	Proximity
Housing	Trunion_Y_port	Displacement, gearbox Y port	mm	Proximity

23

Location	Nomenclature	Expanded Nomenclature	Units	Sensor(s)
Housing	Trunion_X_stbd	Displacement, gearbox X starboard	mm	Proximity
Housing	Trunion_X_port	Displacement, gearbox X port	mm	Proximity
Housing	WEB_STRAIN_0	Strain in carrier web, 0° direction	mV/V	Strain gage
Housing	WEB_STRAIN_45	Strain in web, 45° direction	mV/V	Strain gage
Housing	WEB_STRAIN_315	Strain in web, 315° direction	mV/V	Strain gage
Ring gear	INT_KHB_0_A	Strain, ring gear teeth, 0° location	mV/V	Strain gage
Ring gear	INT_KHB_0_B	Strain, ring gear teeth, 0° location	mV/V	Strain gage
Ring gear	INT_KHB_0_C	Strain, ring gear teeth, 0° location	mV/V	Strain gage
Ring gear	INT_KHB_0_D	Strain, ring gear teeth, 0° location	mV/V	Strain gage
Ring gear	INT_KHB_0_E	Strain, ring gear teeth, 0° location	mV/V	Strain gage
Ring gear	INT_KHB_0_F	Strain, ring gear teeth, 0° location	mV/V	Strain gage
Ring gear	INT_KHB_0_G	Strain, ring gear teeth, 0° location	mV/V	Strain gage
Ring gear	INT_KHB_0_H	Strain, ring gear teeth, 0° location	mV/V	Strain gage
Ring gear	INT_KHB_120_A	Strain, ring gear teeth, 120° location	mV/V	Strain gage
Ring gear	INT_KHB_120_B	Strain, ring gear teeth, 120° location	mV/V	Strain gage
Ring gear	INT_KHB_120_C	Strain, ring gear teeth, 120° location	mV/V	Strain gage
Ring gear	INT_KHB_120_D	Strain, ring gear teeth, 120° location	mV/V	Strain gage
Ring gear	INT_KHB_120_E	Strain, ring gear teeth, 120° location	mV/V	Strain gage
Ring gear	INT_KHB_120_F	Strain, ring gear teeth, 120° location	mV/V	Strain gage
Ring gear	INT_KHB_120_G	Strain, ring gear teeth, 120° location	mV/V	Strain gage
Ring gear	INT_KHB_120_H	Strain, ring gear teeth, 120° location	mV/V	Strain gage
Ring gear	INT_KHB_240_A	Strain, ring gear teeth, 240° location	mV/V	Strain gage
Ring gear	INT_KHB_240_B	Strain, ring gear teeth, 240° location	mV/V	Strain gage
Ring gear	INT_KHB_240_C	Strain, ring gear teeth, 240° location	mV/V	Strain gage
Ring gear	INT_KHB_240_D	Strain, ring gear teeth, 240° location	mV/V	Strain gage

Location	Nomenclature	Expanded Nomenclature	Units	Sensor(s)
Ring gear	INT_KHB_240_E	Strain, ring gear teeth, 240° location	mV/V	Strain gage
Ring gear	INT_KHB_240_F	Strain, ring gear teeth, 240° location	mV/V	Strain gage
Ring gear	INT_KHB_240_G	Strain, ring gear teeth, 240° location	mV/V	Strain gage
Ring gear	INT_KHB_240_H	Strain, ring gear teeth, 240° location	mV/V	Strain gage
Ring gear	EXT_KHB_0_A	Strain, ring gear exterior, 0° location	mV/V	Strain gage
Ring gear	EXT_KHB_0_B	Strain, ring gear exterior, 0° location	mV/V	Strain gage
Ring gear	EXT_KHB_0_C	Strain, ring gear exterior, 0° location	mV/V	Strain gage
Ring gear	EXT_KHB_0_D	Strain, ring gear exterior, 0° location	mV/V	Strain gage
Ring gear	EXT_KHB_0_E	Strain, ring gear exterior, 0° location	mV/V	Strain gage
Ring gear	EXT_KHB_0_F	Strain, ring gear exterior, 0° location	mV/V	Strain gage
Ring gear	EXT_KHB_0_G	Strain, ring gear exterior, 0° location	mV/V	Strain gage
Ring gear	EXT_KHB_0_H	Strain, ring gear exterior, 0° location	mV/V	Strain gage
Ring gear	EXT_KHB_120_A	Strain, ring gear exterior, 120° location	mV/V	Strain gage
Ring gear	EXT_KHB_120_B	Strain, ring gear exterior, 120° location	mV/V	Strain gage
Ring gear	EXT_KHB_120_C	Strain, ring gear exterior, 120° location	mV/V	Strain gage
Ring gear	EXT_KHB_120_D	Strain, ring gear exterior, 120° location	mV/V	Strain gage
Ring gear	EXT_KHB_120_E	Strain, ring gear exterior, 120° location	mV/V	Strain gage
Ring gear	EXT_KHB_120_F	Strain, ring gear exterior, 120° location	mV/V	Strain gage
Ring gear	EXT_KHB_120_G	Strain, ring gear exterior, 120° location	mV/V	Strain gage
Ring gear	EXT_KHB_120_H	Strain, ring gear exterior, 120° location	mV/V	Strain gage
Ring gear	EXT_KHB_240_A	Strain, ring gear exterior, 240° location	mV/V	Strain gage
Ring gear	EXT_KHB_240_B	Strain, ring gear exterior, 240° location	mV/V	Strain gage
Ring gear	EXT_KHB_240_C	Strain, ring gear exterior, 240° location	mV/V	Strain gage
Ring gear	EXT_KHB_240_D	Strain, ring gear exterior, 240° location	mV/V	Strain gage
Ring gear	EXT_KHB_240_E	Strain, ring gear exterior, 240° location	mV/V	Strain gage

Location	Nomenclature	Expanded Nomenclature	Units	Sensor(s)
Ring gear	EXT_KHB_240_F	Strain, ring gear exterior, 240° location	mV/V	Strain gage
Ring gear	EXT_KHB_240_G	Strain, ring gear exterior, 240° location	mV/V	Strain gage
Ring gear	EXT_KHB_240_H	Strain, ring gear exterior, 240° location	mV/V	Strain gage
Carrier	Carrier_047	Displacement, carrier, X direction, 047°	mm	Proximity
Carrier	Carrier_137	Displacement, carrier, X direction, 137°	mm	Proximity
Carrier	Carrier_227	Displacement, carrier, X direction, 227°	mm	Proximity
Carrier	Carrier_317	Displacement, carrier, X direction, 317°	mm	Proximity
Carrier	Radial_040	Displacement Radial 40°	mm	Proximity
Carrier	Radial_310	Displacement Radial 310°	mm	Proximity
Planet	PlanetB_Rim_0	Displacement, X direction, 0°	mm	Proximity
Planet	PlanetB_Rim_90	Displacement, X direction, 90°	mm	Proximity
Planet	PlanetB_Rim_180	Displacement, X direction, 180°	mm	Proximity
Planet	PlanetC_Rim_0	Displacement, X direction, 0°	mm	Proximity
Planet	PlanetC_Rim_90	Displacement, X direction, 90°	mm	Proximity
Planet	PlanetC_Rim_180	Displacement, X direction, 180°	mm	Proximity
Planet	PlanetA_LOAD_UW_70	Strain, Planet A, upwind bearing, 70°	mV/V	Strain gage
Planet	PlanetA_LOAD_UW_160	Strain, Planet A, upwind bearing, 160°	mV/V	Strain gage
Planet	PlanetA_LOAD_UW_250	Strain, Planet A, upwind bearing, 250°	mV/V	Strain gage
Planet	PlanetA_LOAD_UW_340	Strain, Planet A, upwind bearing, 340°	mV/V	Strain gage
Planet	PlanetA_LOAD_DW_20	Strain, Planet A, downwind bearing, 20°	mV/V	Strain gage
Planet	PlanetA_LOAD_DW_115	Strain, Planet A, downwind bearing, 115°	mV/V	Strain gage
Planet	PlanetA_LOAD_DW_200	Strain, Planet A, downwind bearing, 200°	mV/V	Strain gage
Planet	PlanetA_LOAD_DW_285	Strain, Planet A, downwind bearing, 285°	mV/V	Strain gage
Planet	PlanetA_TEMP_UW_OUT1	Temperature, Planet A, upwind bearing, 340°	°C	Thermocouple
Planet	PlanetA_TEMP_UW_IN1	Temperature, Planet A, upwind bearing, 340°	°C	Thermocouple

26

Location	Nomenclature	Expanded Nomenclature	Units	Sensor(s)
Planet	PlanetA_TEMP_DW_IN1	Temperature, Planet A, downwind bearing, 20°	°C	Thermocouple
Planet	PlanetA_TEMP_DW_OUT1	Temperature, Planet A, downwind bearing, 20°	°C	Thermocouple
Planet	PlanetB_LOAD_UW_10	Strain, Planet B, upwind bearing, 10°	mV/V	Strain gage
Planet	PlanetB_LOAD_UW_32	Strain, Planet B, upwind bearing, 32°	mV/V	Strain gage
Planet	PlanetB_LOAD_UW_70	Strain, Planet B, upwind bearing, 70°	mV/V	Strain gage
Planet	PlanetB_LOAD_UW_160	Strain, Planet B, upwind bearing, 160°	mV/V	Strain gage
Planet	PlanetB_LOAD_UW_250	Strain, Planet B, upwind bearing, 250°	mV/V	Strain gage
Planet	PlanetB_LOAD_UW_288	Strain, Planet B, upwind bearing, 288°	mV/V	Strain gage
Planet	PlanetB_LOAD_UW_310	Strain, Planet B, upwind bearing, 310°	mV/V	Strain gage
Planet	PlanetB_LOAD_UW_327.5	Strain, Planet B, upwind bearing, 327.5°	mV/V	Strain gage
Planet	PlanetB_LOAD_UW_340	Strain, Planet B, upwind bearing, 340°	mV/V	Strain gage
Planet	PlanetB_LOAD_UW_352.5	Strain, Planet B, upwind bearing, 352.5°	mV/V	Strain gage
Planet	PlanetB_LOAD_DW_7.5	Strain, Planet B, downwind bearing, 7.5°	mV/V	Strain gage
Planet	PlanetB_LOAD_DW_20	Strain, Planet B, downwind bearing, 20° (assumed to actually be PlanetB_LOAD_DW_285)	mV/V	Strain gage
Planet	PlanetB_LOAD_DW_32.5	Strain, Planet B, downwind bearing, 32.5°	mV/V	Strain gage
Planet	PlanetB_LOAD_DW_50	Strain, Planet B, downwind bearing, 50°	mV/V	Strain gage
Planet	PlanetB_LOAD_DW_77	Strain, Planet B, downwind bearing, 77° (non-operational, assumed equal to PlanetB_LOAD_DW_323)	mV/V	Strain gage
Planet	PlanetB_LOAD_DW_115	Strain, Planet B, downwind bearing, 115°	mV/V	Strain gage
Planet	PlanetB_LOAD_DW_200	Strain, Planet B, downwind bearing, 200°	mV/V	Strain gage
Planet	PlanetB_LOAD_DW_285	Strain, Planet B, downwind bearing, 285° (assumed to actually be PlanetB_LOAD_DW_20)	mV/V	Strain gage
Planet	PlanetB_LOAD_DW_323	Strain, Planet B, downwind bearing, 323°	mV/V	Strain gage
Planet	PlanetB_LOAD_DW_350	Strain, Planet B, downwind bearing, 350°	mV/V	Strain gage
Planet	PlanetB_TEMP_UW_OUT1	Temperature, Planet B, upwind bearing, 340°	°C	Thermocouple

Location	Nomenclature	Expanded Nomenclature	Units	Sensor(s)
Planet	PlanetB_TEMP_UW_IN1	Temperature, Planet B, upwind bearing, 340°	°C	Thermocouple
Planet	PlanetB_TEMP_DW_IN1	Temperature, Planet B, downwind bearing, 20°	°C	Thermocouple
Planet	PlanetB_TEMP_DW_OUT2	Temperature, Planet B, downwind bearing, 20°	°C	Thermocouple
Planet	PlanetC_LOAD_UW_70	Strain, Planet C, upwind bearing, 70°	mV/V	Strain gage
Planet	PlanetC_LOAD_UW_160	Strain, Planet C, upwind bearing, 160°	mV/V	Strain gage
Planet	PlanetC_LOAD_UW_250	Strain, Planet C, upwind bearing, 250°	mV/V	Strain gage
Planet	PlanetC_LOAD_UW_340	Strain, Planet C, upwind bearing, 340°	mV/V	Strain gage
Planet	PlanetC_LOAD_DW_20	Strain, Planet C, downwind bearing, 20°	mV/V	Strain gage
Planet	PlanetC_LOAD_DW_115	Strain, Planet C, downwind bearing, 115°	mV/V	Strain gage
Planet	PlanetC_LOAD_DW_200	Strain, Planet C, downwind bearing, 200°	mV/V	Strain gage
Planet	PlanetC_LOAD_DW_285	Strain, Planet C, downwind bearing, 285°	mV/V	Strain gage
Planet	PlanetC_TEMP_UW_OUT1	Temperature, Planet C, upwind bearing, 340°	°C	Thermocouple
Planet	PlanetC_TEMP_UW_IN1	Temperature, Planet C, upwind bearing, 340°	°C	Thermocouple
Planet	PlanetC_TEMP_DW_IN1	Temperature, Planet C, downwind bearing, 20°	°C	Thermocouple
Planet	PlanetC_TEMP_DW_OUT1	Temperature, Planet C, downwind bearing, 20°	°C	Thermocouple
Sun	Sun_radial_ZZ	Displacement, radial, Z direction	mm	Proximity
Sun	Sun_radial_YY	Displacement, radial, Y direction	mm	Proximity
LSS	Temp_LSS_DW_BRG	Temperature, outer race	°C	RTD
ISS	Temp_ISS_DW_BRG	Temperature, outer race	°C	RTD
HSS	HSS_Speed	Shaft speed	rpm	Calculated
HSS	HSS_Azimuth	Azimuth angle	degrees	Encoder
HSS	HSS_TQ	Torque	mV/V	Strain gage
HSS	TEMP_HSS_TRB_IR_UW	Temperature, upwind TRB inner ring (poor data quality after October 21, 2016)	°C	RTD
HSS	TEMP_HSS_TRB_IR_DW	Temperature, downwind TRB inner ring (poor data quality after October 21, 2016)	°C	RTD

28

Location	Nomenclature	Expanded Nomenclature	Units	Sensor(s)
HSS	TEMP_HSS_TRB_OR_UW	Temperature, upwind TRB outer ring	°C	RTD
HSS	TEMP_HSS_TRB_OR_DW	Temperature, downwind TRB outer ring	°C	RTD
Lube System	ISO_OIL_CLEAN	Oil cleanliness, raw signal	-	CSM 1220
Lube System	ISO_1	Oil cleanliness, bin 1	-	Calculated
Lube System	ISO_2	Oil cleanliness, bin 2	-	Calculated
Lube System	ISO_3	Oil cleanliness, bin 3	-	Calculated
Lube System	Lube_Flow_Pump	Flow rate, total, at lube pump	lpm	Fan speed
Lube System	Lube_Return_Temp	Temperature, oil at main pump	°C	RTD
Lube System	Lube_Flow_Meter	Flow rate, to gearbox, at lube pump	lpm	Flow meter
Lube System	Lube_Fan_Speed	Speed, lube system fan	rpm	Fan speed
Lube System	Lube_Manifold_Pressure	Pressure, oil at distribution manifold	psi	Pressure
Lube System	Lube_Manifold_Temp	Temperature, oil at distribution manifold	°C	RTD
Lube System	Sump_Temp	Temperature, oil in gearbox sump	°C	RTD
Controller	Controller_G_contactor	Large-generator contactor	-	Relay
Controller	Controller_bypass_contactor	Soft-start bypass contactor	-	Relay
Controller	kW	Power, real	kW	Transformer
Controller	kVAR	Power, reactive	kVAR	Transformer

29

Table A-2. Elements of 2,000-Hz Sample Rate Data

Location	Nomenclature	Expanded Nomenclature	Units	Sensor(s)
DAS	MS Excel Timestamp	Time, MS Excel format, from Jan 1, 1900	days	DAS
DAS	LabVIEW Timestamp	Time, Labview format, from Jan 1, 1904	s	DAS
Dyno Motor	Dyno_Speed	Speed, dynamometer gearbox output converted from dynamometer motor	rpm	Calculated
Dyno GB	Dyno_Torque	Torque, dynamometer gearbox output torque spool	kNm	Strain gage
Main shaft	LSS_TQ	Torque	kNm	Strain gage
Main shaft	MSBM_YY	Bending moment, rotating, y-axis	kNm	Strain gage
Main shaft	MSBM_ZZ	Bending moment, rotating, z-axis	kNm	Strain gage
Main shaft	MSBM	Bending moment, total	kNm	Calculated
Main shaft	MSBM_yy	Bending moment, fixed, y-axis	kNm	Calculated
Main shaft	MSBM_zz	Bending moment, fixed, z-axis	kNm	Calculated
Main shaft	LSS_Azimuth	Azimuth angle	degrees	Encoder
Main shaft	LSS_Speed	Shaft speed	rpm	Calculated
HSS	HSS_UY_BM	Bending moment, upwind of mesh, rotating, y-axis	mV/V	Strain gage
HSS	HSS_UZ_BM	Bending moment, upwind of mesh, rotating, z-axis	mV/V	Strain gage
HSS	HSS_DY_BM	Bending moment, downwind of mesh, rotating, y-axis	mV/V	Strain gage
HSS	HSS_DZ_BM	Bending moment, downwind of mesh, rotating, z-axis	mV/V	Strain gage
HSS	HSS_exY_BM	Bending moment, downwind of bearings, rotating, y-axis	mV/V	Strain gage
HSS	HSS_exZ_BM	Bending moment, downwind of bearings, rotating, z-axis	mV/V	Strain gage
HSS	HSS_TQ	Torque	mV/V	Strain gage
HSS	TEMP_HSS_TRB_IR_UW	Temperature, upwind TRB inner ring (poor data quality after October 21, 2016)	°C	RTD
HSS	TEMP_HSS_TRB_IR_DW	Temperature, downwind TRB inner ring (poor data quality after October 21, 2016)	°C	RTD
HSS	TEMP_HSS_TRB_OR_UW	Temperature, upwind TRB outer ring	°C	RTD

30

Location	Nomenclature	Expanded Nomenclature	Units	Sensor(s)
HSS	TEMP_HSS_TRB_OR_DW	Temperature, downwind TRB outer ring	°C	RTD
HSS	HSS_Speed	Shaft speed	rpm	Calculated
HSS	HSS_Azimuth	Azimuth angle	degrees	Encoder
Controller	Controller_G_contactor	Large-generator contactor	-	Relay
Controller	Controller_bypass_contactor	Soft-start bypass contactor	-	Relay
Controller	kW	Power, real	kW	Transformer
Controller	kVAR	Power, reactive	kVAR	Transformer

ENGINEERING-PDH.COM
| MEC-151 |